Microscopic and Microbial Insights into the Stony Coral Tissue Loss Disease (SCTLD) Outbreak Across Multiple Coral Species on Florida's Coral Reef

Florida Department of Environmental Protection
Coral Reef Conservation Program (CRCP) Project 11

Microscopic and Microbial Insights into the Stony Coral Tissue Loss Disease (SCTLD) Outbreak Across Multiple Coral Species on Florida's Coral Reef

Final Report

Prepared By:
Jennifer L. Salerno PhD
Esther C. Peters PhD

George Mason University
Department of Environmental Science and Policy
4400 University Drive, MS 5F2
Fairfax, VA 22030-4444

August 31, 2020

Completed in Fulfillment of PO B67289 for

Florida Department of Environmental Protection
Coral Reef Conservation Program
1277 N.E. 79th Street Causeway
Miami, FL 33138

This report should be cited as follows:
Salerno, J.L., and Peters, E.C. 2020. Microscopic and Microbial Insights into the Stony Coral Tissue Loss Disease (SCTLD) Outbreak Across Multiple Coral Species on Florida's Coral Reef. Florida DEP. Miami, FL. Pp. 42.

This report was prepared for the Florida Department of Environmental Protection, Office of Resilience and Coastal Protection by George Mason University. Funding was provided by the Florida Department of Environmental Protection and the National Oceanic and Atmospheric Administration (NOAA) Coral Reef Conservation Program. The views, conclusions and recommendations expressed herein are those of the authors and do not necessarily reflect the views of the State of Florida, NOAA or any of its sub-agencies.

Cover Photo: Esther C. Peters

Executive Summary

Three integrated research tasks were performed using molecular biology, histology, and immunohistochemistry to provide insights into a possible mechanism of bacterial infection that results in tissue loss, as well as potential pathogen(s) associated with stony coral tissue loss disease (SCTLD). For Task 1, molecular tools were used to characterize the endolithic communities of fungi, bacteria, and archaea from apparently healthy coral colonies, and affected and unaffected portions of diseased colonies sampled in 2016 and 2017. For Task 2 histological methods were used to characterize the endosymbiotic dinoflagellates in mucus and tissue from healthy, diseased, and unaffected portions of colonies and examine their role in the pathogenesis of SCTLD. For Task 3 immunohistochemistry was used to investigate the role of programmed cell death (PCD) vs. necrosis in SCTLD. Due to time constraints imposed by COVID-19-associated laboratory closures, further work is needed.

Preliminary results from Task 1 revealed that the endolithic coral microbiome (bacteria and fungi) varied in community composition based primarily on host coral species and then disease state, especially regarding the fungal microbiome. Additional sample replicates and bioinformatic analyses will be performed to further investigate specific microbes driving these observed differences, as well as the functional potential of the coral microbiome during different disease states. Preliminary results from Task 2 showed that dinoflagellate abundance was reduced in the gastrodermis of most of the 2016 samples examined and remaining zooxanthellae were often degraded or lysing in the apparently healthy, diseased, and unaffected tissue samples from all four species of coral. Liquefactive necrosis was observed in all species, with few to no zooxanthellae in these lesions that were usually restricted to the gastrodermal tissue with the mesoglea and epidermis remaining intact. Gastrodermis adjacent to these lesions included pale-staining algal cells with vacuolation, swelling, then cell wall disintegration and lysing (ghosting). Preliminary results from Task 3 revealed apoptosis was consistently observed in tissues of SCTLD-affected corals, indicating that this mode of cell death is involved in SCTLD pathology. However, apoptosis was also observed in some tissue without an apparent lesion, indicating that apoptosis may be an early indicator of disease before degradation can be detected morphologically. Additional samples and further analysis are needed to understand normal apoptosis involved in cell replacement and fully describe the interplay between the mechanism of cell death and other histological indicators of SCTLD.

Continuation of this project will utilize the full sample set to better understand disease mechanisms and to identify potential pathogenic agents involved in the progression of SCTLD in reef-building corals.

Acknowledgements

The 2016 and 2017 frozen core samples and unstained histoslides cut from tissues embedded in paraffin blocks were provided by Florida's Fish and Wildlife Research Institute (FWRI). We are grateful to Drs. Jan Landsberg and Yasu Kiryu, and Lindsay Huebner of FWRI, as well as Drs. Erinn Muller, Abigail Clark, and Katie Eaton of Mote Marine Laboratory, for coordinating shipping of the samples to us. Coral sample collections were made with funding support from the U.S. Fish and Wildlife Service through the State Wildlife Grants Program and the Florida Department of Environmental Protection's Coral Reef Conservation Program from the Southeast Florida Coral Reef Ecosystem Conservation Area and the Florida Keys National Marine Sanctuary.

Table of Contents

List of Figures

List of Tables

List of Acronyms and Abbreviations

BBW	basal body wall
BLASTn	Basic Local Alignment Search Tool - nucleotide
CIBs	crystalline inclusion bodies
CNAT	*Colpophyllia natans*
COVID-19	coronavirus disease started in 2019 caused by the virus SARS-CoV-2
DEP	Florida Department of Environmental Protection
DLAB	*Diploria labyrinthiformis*
DNA	deoxyribonucleic acid
dUTP	2'-deoxyuridine 5'-triphosphate
FCR	Florida's Coral Reef
FISH	fluorescent in situ hybridization
FWC	Florida Fish and Wildlife Conservation Commission
FWRI	Florida's Fish and Wildlife Research Institute
GMU	George Mason University
g	gram(s)
H&E	hematoxylin and eosin
h	hour(s)
HIER	heat-induced epitope retrieval
IHC	immunohistochemistry
ITS	internal transcribed spacer region
LCM	laser capture microdissection
LN	liquefactive necrosis
MCAV	*Montastraea cavernosa*
min	minute(s)
µL	microliter(s)
µM	micromolar
mL	milliliter(s)
mM	millimolar
MML	Mote Marine Laboratory
NASA	National Aeronautics and Space Administration
NOAA	National Oceanic and Atmospheric Administration
NSU	Nova Southeastern University
OFAV	*Orbicella faveolata*
PAST	*Porites astreoides*
PBS	Phosphate-buffered saline
PCD	Programmed cell death
PCLI	*Pseudodiploria strigosa*
PIER	proteolytic-induced epitope retrieval
s	second(s)
SBW	surface body wall
SCTLD	stony coral tissue loss disease
SRA	Sequence Read Archive
SSID	*Siderastrea siderea*
SWG	State Wildlife Grant

List of Acronyms and Abbreviations, Continued

RSMAS	Rosenstiel School of Marine and Atmospheric Science
TdT	terminal deoxynucleotidyl transferase
TUNEL	terminal deoxynucleotidyl transferase dUTP nick end labeling
URL	universal resource locator
WP	white plague

1. INTRODUCTION

Florida's Coral Reef (FCR) is currently experiencing a multi-year disease-related mortality event that has resulted in massive die-offs in multiple coral species (Precht et al. 2016, Walton et al. 2018). Approximately 21 species of coral, including both Endangered Species Act-listed and the primary reef-building species, have displayed tissue loss lesions that often result in whole colony mortality. First observed near Virginia Key in late 2014, the disease has since spread to the northernmost extent of the FCR, and south to the Marquesas in the Lower Florida Keys (Florida Department of Environmental Protection, https://floridadep.gov/rcp/coral/content/stony-coral-tissue-loss-disease-response), as well as to multiple distant sites in the northern Caribbean Sea (Atlantic and Gulf Rapid Reef Assessment, https://www.agrra.org/coral-disease-outbreak/).

Preliminary evidence indicated that bacteria play a role in the disease process (as discussed during the SCTLD Technical Workshop in June 2019); however, the causative agent of the disease has not yet been identified and multiple factors may be involved. Observations made by Drs. Jan Landsberg and Yasu Kiryu (Florida Fish and Wildlife Conservation Commission [FWC] and the Fish and Wildlife Research Institute [FWRI]) during their histopathological examinations of coral samples collected in 2016 and 2017, indicated that focused studies of the roles played by zooxanthellae, apoptosis, and endolithic microorganisms in the pathogenesis of SCTLD were warranted.

The 2016–2017 samples are among the earliest collected for both histopathology and microbiology analyses, but with duplicate cores (comprised of coral skeleton, tissue, and mucous layer) collected for each sample type (healthy colonies and affected and unaffected portions of diseased colonies). One core was fixed in either formaldehyde or glutaraldehyde solution for light and transmission electron microscopy, respectively, and one was frozen for molecular studies of the microbiome. The biopsy cores from the 2016–2017 sampling effort were archived at -80 ℃ at FWRI. In 2018, a more extensive sampling effort was conducted by FWRI staff to obtain biopsy cores for histopathological examination, as well as surface mucus/tissue scrapings collected using a syringe technique for molecular microbiological analyses. These samples became the focus of a study funded by a State Wildlife Grant (SWG) to Drs. Landsberg and Kiryu with Dr. Erinn Muller, Mote Marine Laboratory (MML), and Dr. Esther Peters, George Mason University (GMU). In addition to studying the samples for histopathological changes and microorganisms, genomic DNA from surface mucus/tissue samples was extracted by Drs. Muller and Abigail Clark at MML, processed, and sequenced to identify bacteria. In September 2019, Lindsay Huebner (FWRI), Dr. Muller, and Dr. Kim Ritchie (University of South Carolina at Beaufort) were awarded a U.S. Environmental Protection Agency grant to include the processing of the 2016–2017 frozen samples, replicating the method used on the 2018 field-collected syringe samples to collect surface mucus/tissue scrapings, extract the DNA, and sequence for microbial characterization (Bacteria and Archaea). These results will be compared with the histopathological results to help identify pathogenic microorganisms that may include the primary SCTLD-causing agent(s). The histopathology samples embedded in paraffin blocks are archived by Drs. Landsberg and Kiryu at FWRI. They have provided additional

unstained tissue sections mounted on glass microscope slides for fluorescent in situ hybridization (FISH) and laser capture microdissection (LCM) assays conducted in Dr. Peters' laboratory.

1.1. Proposed Research

Our interest in surveying the coral skeletal portions of the samples stemmed from observations that tissue damage and suspect bacteria or viruses (crystalline inclusion bodies, CIBs) have been found in the basal body wall of the coenenchyme and the polyp deep in the corallite, which may not be captured by surface scrapings (Figure 1). Three additional findings from the histopathological examinations performed by FWRI and GMU indicated that additional biotic or abiotic factors should also be considered in the pathogenesis of SCTLD. First, microscopic fungal hyphae that bore through the aragonite exoskeleton of the coral have been seen near the coral tissue in decalcified sections and are often associated with bacteria or archaea. This microbial consortium may release toxins that weaken the corals' immune responses or kill coral cells—alternatively, the degeneration of diseased coral tissue may alter the species in the endolithic community or their relative abundances. Second, the symbiotic dinoflagellates that live in the gastrodermal cells of the corals' polyps are degenerating some distance away from the tissue-loss margins, suggesting that they are more sensitive to a damaging factor than the corals' cells. Furthermore, genotype analyses of these algal cells from the coral species affected by the disease indicate that they largely belong to one genus, *Breviolum* (formerly Clade B). Are the algal cells involved in the coral tissue changes due to their susceptibility to biotic or abiotic pathogen(s) that reduce their ability to provide nutrients and waste recycling in the symbiosis? The third observation of note was that the affected corals variably display pathologic tissue changes that may be identified as necrosis (cell death) or apoptosis (programmed cell death, in which an enzyme cascade is triggered that destroys the cell and can be identified using immunohistochemical techniques). Understanding which of these changes is present (or whether both may occur in the same sample) can aid in our interpretation of the histopathological observations and pathogenesis related to potentially different etiological agents, or the disruption of the dinoflagellate symbiosis that is so important to the functioning of tropical reef-building coral species.

The overarching goal of this work was to investigate the roles of these three histopathological findings in the development of SCTLD. To date, the majority of coral microbiome studies have employed molecular methods that use a homogenized slurry of coral mucus, tissue, and/or skeleton in varying combinations—providing information on the taxonomic composition of the whole microbial community—but resulting in the loss of spatial information with respect to the location of microbes on, or within, the coral host. Conversely, traditional histological techniques provide information on the tissue condition, inferred health state of the host, and location/presence of putative pathogens, but cannot confirm the taxonomic identification of microorganisms or identify other pathogens that may be involved. The information from both methods can be used to develop specific molecular probes to localize putative pathogens in relation to the coral host using FISH paired with epifluorescence microscopy.

Traditional histological techniques are also limited in that they allow for the diagnosis of cellular abnormalities based on morphological observations alone, which can miss the earliest stages of

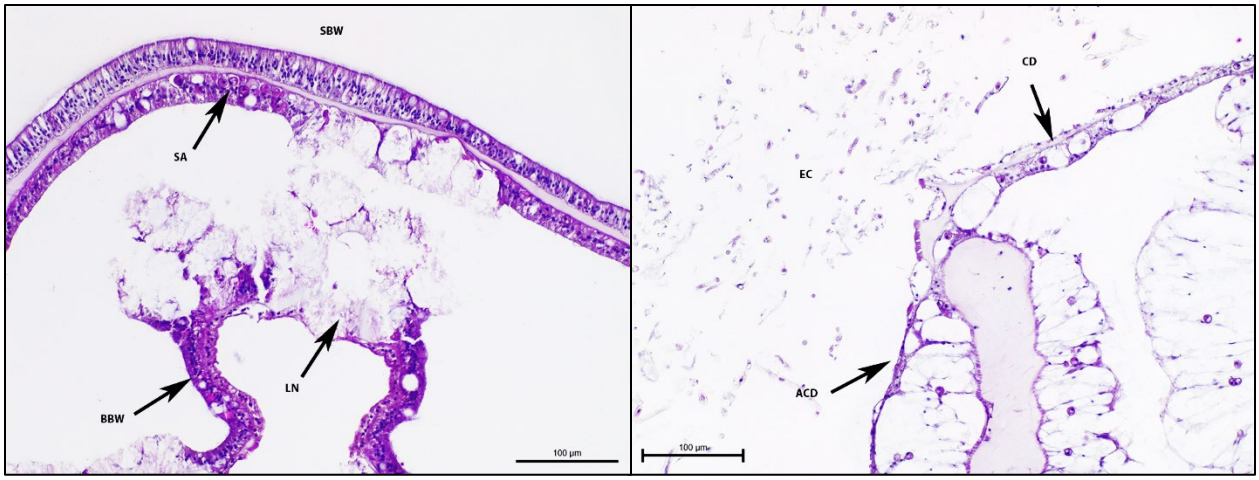

Figure 1: Histopathology observations in SCTLD. Left, middle right arrow liquefactive necrosis (LN) of the basal body wall (BBW) and surface body wall (SBW) gastrodermis in gastrovascular canal tissue covering the coenosteum in *Montastraea cavernosa* 107HD, 2016, Broward County 4, 20x, hematoxylin and eosin (H&E) staining. Upper arrow is pointing to degenerating symbiotic algae in surface body wall gastrodermis; lower left arrow is pointing to BBW where crystalline inclusion bodies and some suspect bacteria have been found. Right, endolithic community (EC) where the skeleton was removed adjacent to *Colpophyllia natans* tissue, 21U, 2016, Grecian Rocks, 20x, H&E. Note at upper arrow the calicodermis (CD) is sloughing, lower arrow points to atrophied or absent calicodermis (ACD).

malfunction before cells begin to degrade, causing a critical gap in spatial information regarding disease pathogenesis within the tissues. Conversely, immunohistochemistry (IHC) can target and highlight specific molecules within cells, providing sensitive and otherwise undetectable information about cell behavior before morphological changes. In the case of cell death, which is of particular interest in the SCTLD lesion of rapid tissue loss, IHC is a useful technique for distinguishing between necrosis and programmed cell death (PCD), which is difficult to identify by morphology alone. The TUNEL (terminal deoxynucleotidyl transferase dUTP nick-end labeling) technique enzymatically labels the free 3'-OH termini of fragmented single- and double-stranded DNA that occur during the early stages of PCD, allowing the visualization of apoptotic cells even before any morphological changes take place. Likewise, while histological observations can identify morphological changes within zooxanthellae, using sequencing data to identify dominant algal symbionts within diseased, unaffected, and healthy coral samples could provide evidence for species susceptibility. Alone, each of these methods present limitations and problematic data gaps, but when combined, provide a promising strategy to identify the causative agent(s) of SCTLD and to characterize the effects of the disease on the coral host.

1.2. Project Goals and Objectives

The outcomes of this project will be incorporated into the on-going coral disease response effort that seeks to improve understanding about the scale and severity of the FCR coral disease outbreak, identify primary and secondary causes, identify management actions to remediate disease impacts, restore affected resources and, ultimately, prevent future outbreaks. The project goals were to (1) use a combination of microscopy and molecular techniques to perform a targeted characterization of the coral microbiome (dinoflagellate endosymbionts, fungi, bacteria,

and archaea) in affected and unaffected portions of diseased colonies to document the effects of the disease on the coral microbiome and to potentially identify the causative agent(s) of stony coral tissue loss disease and (2) to investigate the role of programmed cell death (PCD) in SCTLD pathogenesis to determine whether this immune pathway is utilized by the coral host to respond to pathogens and ultimately contributes to the rapid tissue-loss lesion. Samples previously collected from numerous locations along the FCR in 2016, 2017, and 2018 and processed for histology and genetic studies (extracted DNA) or stored frozen and available for additional molecular work were used. The Methods and Results sections refer to the following tasks:

Task 1: Characterize the endolithic communities of fungi, bacteria, and archaea from apparently healthy coral colonies, and affected and unaffected portions of diseased colonies sampled in 2016 and 2017.

Task 2: Characterize the endosymbiotic dinoflagellates in mucus and tissue from healthy, diseased, and unaffected portions of colonies and examine their role in the pathogenesis of SCTLD.

Task 3: Determine the role of programmed cell death (PCD) vs. necrosis in SCTLD.

2. METHODS

2.1. Task 1: Characterize the endolithic communities of fungi, bacteria, and archaea from apparently healthy coral colonies, and affected and unaffected portions of diseased colonies sampled in 2016 and 2017.

2.1.1 Sample Acquisition

Frozen core samples (51) from 2016 and 2017 were acquired from archived samples prepared by FWRI during their 2016–2018 sampling effort (Table 1). Samples were shipped frozen from MML in Sarasota, Florida, arriving at GMU's Potomac Environmental Research and Education Center, Woodbridge, Virginia, on March 18, 2020. Samples included apparently healthy, diseased, and unaffected tissues (Figure 2). Apparently healthy tissue was collected from coral colonies showing no gross lesions. Diseased and unaffected tissues came from the same colony, with diseased coming from an area along a disease margin and unaffected from an area that was not grossly showing disease. Species included *Colpophyllia natans* (CNAT), *Diploria labyrinthiformis* (DLAB), *Montastraea cavernosa* (MCAV), *Porites astreoides* (PAST), *Pseudodiploria clivosa* (PCLI), *Orbicella faveolata* (OFAV), and *Siderastrea siderea* (SSID). Samples were obtained from one of three locations Martin County, Grecian Rocks, or Dustan Rocks.

2.1.2 DNA Extraction

Prior to processing, samples were photographed using an iPhone X (Apple Inc.) for future reference. Samples were ground using sterile ceramic mortars and pestles. DNA was extracted

Table 1: Complete Task 1 bacterial/archaeal microbiome (not boldface) and fungal microbiome **(boldface)** sample list with numbers of samples per species, collection site, collection date,

condition, and processing status (extracted and sequenced). D = Diseased, U = Unaffected, AH = Apparently Healthy.

Species	Collection Site	Collection Date	D	D	U	U	AH	AH
			Extract.	Seq.	Extract.	Seq.	Extract.	Seq.
CNAT	Grecian Rocks	2016	3 **3**	2 **3**	3 **3**	3 **3**	1 **1**	0 **1**
CNAT	Dustan Rocks	2017					3 **3**	2 **2**
DLAB	Grecian Rocks	2016	2 **2**	1 **0**	2 **2**	1 **1**	1 **1**	0 **0**
DLAB	Dustan Rocks	2017					4 **4**	2 **1**
PCLI	Martin County	2017					2 **2**	0 **0**
MCAV	Grecian Rocks	2016	3 **3**	0 **1**	3 **3**	0 **0**	1 **1**	0 **0**
MCAV	Martin County	2017					6 **6**	1 **1**
MCAV	Dustan Rocks	2017					3 **3**	0 **0**
OFAV	Dustan Rocks	2017					4 **4**	3 **3**
PAST	Martin County	2017					2 **2**	2 **2**
SSID	Martin County	2017					5 **5**	3 **4**
SSID	Dustan Rocks	2017					3 **3**	1 **3**
Totals	**All Sites**	**All Dates**	8 **8**	3 **4**	8 **8**	4 **4**	35 **35**	14 **17**

using QIAGEN's DNeasy® PowerSoil® Kit with the following modifications. Approximately 0.75 grams (g) of tissue from each sample was added to each Powerbead tube. Powerbead tubes were placed in an Omni Bead Ruptor 24 (Omni International, Inc.) for 45 seconds (s) rather than vortexing for 10 minutes (min). Lastly, DNA was eluted by adding 75 microliters (µL) of DEPC water to the white filter membrane of the spin column. After extraction, DNA was stored at -80 °C for further analysis.

2.1.3 Polymerase Chain Reaction (PCR) Amplification of Bacterial, Archaeal, and Fungal Marker Genes

Prior to PCR amplification, extracted genomic DNA was quantified using a Qubit® 2.0 Fluorometer (Invitrogen Life Technologies) according to the manufacturer's protocol. All PCR

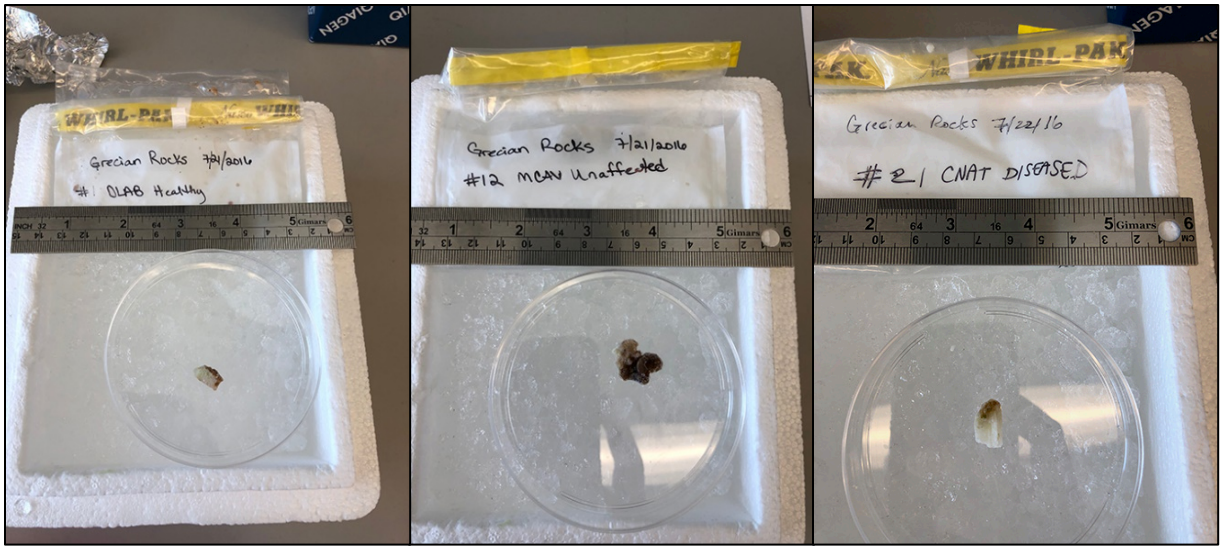

Figure 2: Examples of the frozen core samples used in this project.

reactions were carried out in duplicate. For 16s rRNA gene amplicon-based characterization, Primers 515F (5'-GTG YCA GCM GCC GCG GTA A-3'; Parada et al. 2016) and 806R (5' GGA CTA CNV GGG TWT CTA AT-3'; Apprill et al. 2015) were used to target bacteria and archaea. A PCR master mix was prepared by adding the following per reaction: 5.9 µL of DEPC water, 2 µL of 10X PCR Gold Buffer (Applied Biosystems™ by Life Technologies™) for AmpliTaq Gold polymerase, 2 µL of 25 millimolar (mM) Mg mix and 2 µL of 0.1% bovine serum albumin (BSA), 0.1 µL of AmpliTaq Gold polymerase (5 units/µL), 2 µL of 2 mM each deoxynucleotide triphosphates (dNTPs), and 1 µL of both the forward and reverse primer in a 10 micromolar (µM) concentration. Master mix was aliquoted into 0.2-mL PCR tubes along with 4 µl of extracted DNA from each sample. DNA amplification was performed in a 20 µl final volume solution per reaction.

For fungal characterization, fungal-specific primers ITS1-F (5'CTT GGT CAT TTA GAG GAA GTA A-3'; Gardes and Bruns 1993) and ITS2 (5'- GCT GCG TTC TTC ATC GAT GC-3'; White et al. 1990) were used to amplify the internal transcribed spacer region 1 (ITS1) from the extracted DNA. A PCR master mix was prepared by adding 7.9 µL of DEPC water, 2 µL of 10X PCR Gold Buffer (Applied Biosystems™ by Life Technologies™) for AmpliTaq Gold polymerase, 2 µL of 25 millimolar (mM) Mg mix, 2 µL of 2 mM each deoxynucleotide triphosphates (dNTPs), 1 µL of both the forward and reverse primer in a 10 micromolar (µM) concentration, 2 µL of 0.1% bovine serum albumin, and 0.1 µL AmpliTaq Gold polymerase (5 units/µL) per sample, to a 1.5 milliliter (mL) Eppendorf tube. Master mix (18 µL) was aliquoted into 0.2-mL PCR tubes along with 2 µl of extracted DNA from each sample. DNA amplification was performed in a 20 µl final volume solution per reaction.

All PCR amplifications were carried out on an Applied Biosystems® Veriti 96-well Thermal Cycler (Life Technologies, Frederick, MD). PCR conditions for 16s rRNA gene amplification were as follows: initial denaturation at 95 °C for 3 min; 30 cycles at 95 °C for 30 s, 65 °C for 60 s with each successive cycle reduced by 0.5°C, and primer extension at 72 °C for 2 min; and 1 cycle of 95°C for 30 s, 50°C for 60 s, and 72°C for 20 min. Reactions were then cooled and

stored frozen at -20°C. PCR conditions for ITS gene amplification were as follows: initial denaturation at 95 °C for 11 min; 35 cycles at 95 °C for 30 s, 50 °C for 30 s, 72 °C for 2 min +5 s per cycle; and 1 cycle of 72 °C for 30 min (White et al. 1990). Reactions were then cooled and stored frozen at -20 °C. All PCR products were visualized on a 1% agarose gel in Tris-Acetate-ethylenediaminetetraacetic acid with Invitrogen SYBR® Safe DNA gel stain.

2.1.4 Sequencing and Bioinformatic Analysis

All PCR products were cleaned using the QIAquick PCR Purification Kit (Qiagen), quantified with the Qubit® 2.0 fluorometer, then 500 ng of purified PCR product per sample was sent to the Genewiz® sequencing facility (South Plainfield, NJ) for amplicon sequencing on an Illumina MiSeq platform (Illumina Inc., San Diego, CA, USA). Due to methodological issues with obtaining enough DNA for sequencing (specific to certain species of coral), approximately 50% of extracted samples were sent for sequence analysis. For metagenomic characterization, 1500 ng of genomic DNA template per sample from selected extracted cores (as described above) were sent to Genewiz® for sequencing on an Illumina NextSeq 550 platform (Illumina Inc., San Diego, CA, USA). Raw Fastq files were received from Genewiz® and analyzed using the QIIME2 bioinformatic pipeline (Version 2020.6). Sequences were demultiplexed and denoised, and paired-end reads were trimmed, checked for chimeras, grouped into amplicon sequence variants (ASV) using DADA2 (Callahan et al. 2016, Callahan et al. 2017), aligned with representative sequences using MAFFT (Katoh et al. 2002), and assigned taxonomy using a classifier trained on either SILVA (138 99% OTUs from 515F/806R) or UNITE (DOI: 10.15156/BIO/786385) reference databases for 16S rRNA or ITS gene amplicons, respectively. Alpha diversity indices, on rarefied sequences (Shannon and evenness) were calculated for samples. Beta diversity was calculated using Bray-Curtis dissimilarity (abundance of taxa) to compare differences across samples. Relative abundances of taxa were summarized across samples and displayed using bar plots.

2.2. Task 2: Characterize the endosymbiotic dinoflagellates in mucus and tissue from healthy, diseased, and unaffected portions of colonies and examine their role in the pathogenesis of SCTLD.

2.2.1 Sample Acquisition

Samples (86) were acquired from archived slides prepared by FWRI during the 2016–2018 sampling effort (Table 2). Prepared slides for each sample from 2016 included three serial sections stained with Mayer's hematoxylin and eosin (H&E), thionin, and Giemsa. The 2017–2018 slides that FWRI provided only consisted of block sections stained with Mayer's H&E. The samples included apparently healthy, diseased, and unaffected tissues. Apparently healthy tissue was collected from coral colonies showing no gross lesions. Diseased and unaffected tissues came from the same colony, with diseased coming from an area along a tissue-loss margin and unaffected from an area that was not grossly showing tissue loss. Species included DLAB, MCAV, SSID, and OFAV.

Table 2: Complete Task 2 sample list with species, collection site, collection date, and condition.

Species	Collection Site	Collection Date	Diseased	Unaffected	Apparently Healthy
Colpophyllia natans	Dustan Rocks	April 2017	0	0	3
		Total	**0**	**0**	**3**
Diploria clivosa	Martin County	April 2017	0	0	2
		Total	**0**	**0**	**2**
Diploria labyrinthiformis	Dustan Rocks	April 2017	0	0	5
		Total	**0**	**0**	**5**
Montastraea cavernosa	Broward County 4	November 2016	10	9	8
Montastraea cavernosa	Grecian Rocks	July 2016	4	3	1
Montastraea cavernosa	Dustan Rocks	April 2017	0	0	3
Montastraea cavernosa	Martin County	April 2017	0	0	5
Montastraea cavernosa	Site B-Boot Key	April 2018	2	2	1
		Total	**16**	**14**	**18**
Orbicella faveolata	Broward County	November 2016	2	3	2
Orbicella faveolata	Site B-Boot Key	April 2018	2	2	1
		Total	**4**	**5**	**3**
Porites astreoides	Martin County	April 2017	0	0	2
		Total	**0**	**0**	**2**
Siderastrea siderea	Broward County 4	November 2016	2	3	0
Siderastrea siderea	Grecian Rocks	July 2016	3	3	1
Siderastrea siderea	Martin County	April 2017	0	0	5
		Total	**5**	**6**	**6**
Grand Total	**All Sites**	**All Dates**	**25**	**25**	**36**

2.2.2 Methods

Histological observations were undertaken systematically, beginning with examining dinoflagellate condition in the opportunistically collected 2016 samples and moving towards the proposed creation of new histoslides (if time allowed) from recently collected coral cores that Dr. Andrew Baker's team at the University of Miami, Rosenstiel School of Marine and Atmospheric Sciences, planned to manipulate to contain the dinoflagellates from the genera *Breviolum*, *Durusdinium*, or no dinoflagellates at all, and then expose them to diseased coral fragments. This schedule was designed to build a foundation of knowledge so that similarities or differences can be more readily identified as the experimental samples become available. The Baker samples will also be analyzed molecularly to confirm dinoflagellate classification and transcriptomics, which will then be complemented by the histopathological observations, allowing for more in-depth interpretation of what occurs in SCTLD pathogenesis. Dr. Baker's samples were not received during this project, so no results from that are included in this report.

Microscopic characterization of the endosymbiotic dinoflagellates (zooxanthellae) was undertaken using an Olympus BX43 Clinical Microscope with an attached Olympus DP72 camera. Photomicrographs were taken using CellSens software and 100x objective with immersion oil. Gastrodermal tissue was located and ten photomicrographs of the surface body wall (SBW) were taken at random along its length of the tissue on each histoslide. More than 970 individual photos were taken from the slides provided by FWRI. Extra photos were taken for clarification when multiple depths of field made it difficult to identify the actual number of zooxanthellae.

Using ImageJ (Rasband 2020), dinoflagellate counts, total and number dividing, were conducted in 50-micron segments for each micrograph (Figure 3). Gastrodermal length and thickness were also measured. Averages were calculated for total number of dinoflagellates, percent dividing, and gastrodermal thickness. Total gastrodermal length observed for each slide was also calculated.

Presence of necrosis, degradation, and crystalline inclusion bodies (CIBs) were scored on a 0 (no) or 1 (yes) scale for every slide. Necrosis criteria included coagulative, liquefactive, and pyknotic. Degradation criteria included presence of gold-brown dinoflagellates, lysing dinoflagellates ("ghosts"), melanin, vacuolated dinoflagellates, swollen dinoflagellates, and dinoflagellates containing uric acid crystals.

Due to lab closures caused by the COVID-19 pandemic, only 54 histoslides out of 65 total received from the 2016 samples were examined and scored for necrosis, degradation, and the presence of CIBs. These included subsets from each of the four species provided by FWRI.

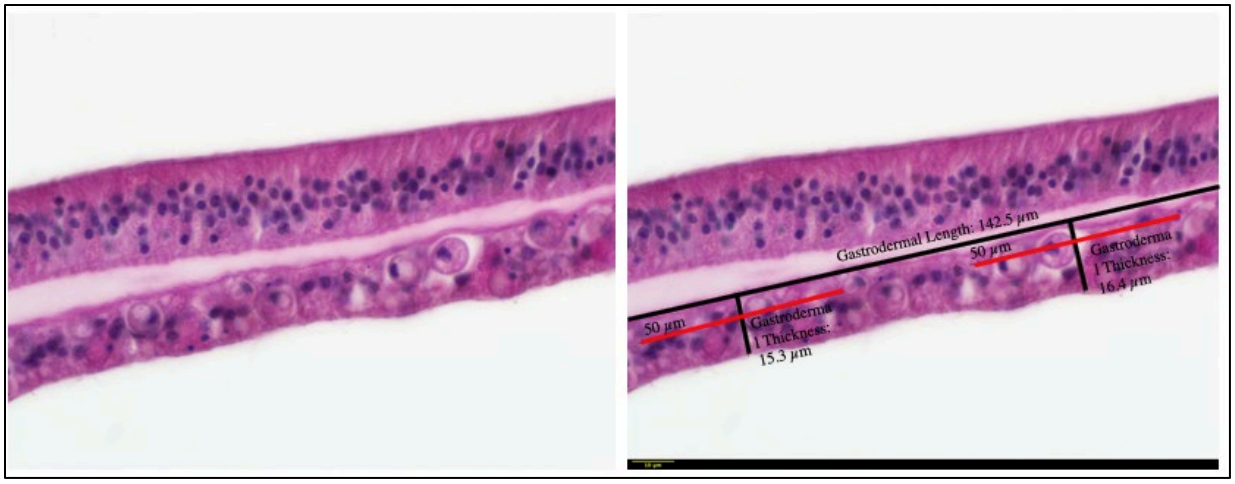

Figure 3: Measurements taken for MCAV 1H using ImageJ before and after. Scale bar was added using the Scale Bar Tools for Microscopes plugin. Gastrodermal length followed the widest path of the gastrodermis for consistency. Gastrodermal thickness was taken for each 50-μm section and an average thickness was calculated.

2.3. Task 3: Determine the role of programmed cell death (PCD) vs. necrosis in SCTLD.

2.3.1 Sample Acquisition

Tissue sections were prepared from the tissue core samples archived at FWRI and collected during the same 2016–2018 sampling effort. To overcome delays and limitations imposed by the COVID-19 pandemic, samples were also acquired opportunistically from ongoing SCTLD projects (Table 3) in the Florida Keys conducted by Dr. Karen Neely and in Broward County conducted by Drs. David Gilliam, Brian Walker, and Joana Figueiredo (NSU). Diseased tissue cores were taken from the active tissue-loss margins of corals with SCTLD, unaffected tissue cores were taken from the apparently healthy portions of a colony with an active SCTLD lesion, and apparently healthy tissue cores were taken from corals with no visible signs of tissue loss.

2.3.2 Sample Processing for Histology and Immunohistochemistry

All samples collected separately from the FWRI-archived collection were fixed in either a solution of 1 part Z-Fix Concentrate (Anatech, Ltd.) diluted with 4 parts filtered seawater or 4%

paraformaldehyde (w/v) in phosphate buffered saline (PBS) for a minimum of 20 h. Diseased tissues were enrobed in agarose gel to preserve structure during further processing steps. All samples were decalcified in 10% EDTA and then embedded in paraffin blocks for sectioning onto glass slides. Serial tissue sections were taken from each block, half to be stained with Mayer's hematoxylin and eosin for general tissue structure, and half to be stained using immunohistochemical techniques for apoptosis.

Table 3: Complete Task 3 sample list with species, collection site, collection date, and condition.

Species	Collection Site	Collection Date	Diseased	Unaffected	Apparently Healthy
Pseudodiploria strigosa	Lower Keys	June 2019	4	0	0
Pseudodiploria strigosa	East Turtle Shoal	April 2018	2	2	1
Pseudodiploria strigosa	West Turtle Shoal	April 2018	0	0	1
Pseudodiploria strigosa	Broward County	February 2020	0	0	1
		Total	**6**	**2**	**3**
Montastraea cavernosa	West Turtle Shoal	April 2018	2	2	1
Montastraea cavernosa	East Turtle Shoal	April 2018	0	0	1
Montastraea cavernosa	Broward County	July 2020	0	0	3
		Total	**2**	**2**	**5**
Orbicella faveolata	West Turtle Shoal	April 2018	1	1	1
Orbicella faveolata	East Turtle Shoal	April 2018	0	0	1
Orbicella faveolata	Dustan Rocks	April 2018	0	0	1
		Total	**1**	**1**	**3**
Dichoceonia stokesii	Lil Hope	February 2020	1	1	0
		Total	**1**	**1**	**0**
Colpophyllia natans	Lil Hope	February 2020	1	1	0
		Total	**1**	**1**	**0**
Orbicella annularis	Lil Hope	February 2020	1	1	0
		Total	**1**	**1**	**0**
Grand Total	**All Sites**	**All Dates**	**12**	**8**	**11**

The Apoptag in situ Apoptosis Detection Kit (Millipore Sigma) was used to highlight areas of apoptosis in paraffin-embedded coral tissues, which uses the TUNEL method (terminal deoxynucleotidyl transferase dUTP nick-end labeling) to stain the fragmented DNA ends associated with this process. Tissue sections were first dewaxed in xylene and rehydrated in a series of alcohols before being treated for epitope retrieval, which breaks the protein crosslinks that are formed during fixation to expose the antigens that will facilitate DNA labelling. After treatment for epitope retrieval (either incubation with a digestive enzyme, heated incubation with

a buffer, or incubation with a detergent, see below in Methods Development section), sections were washed in phosphate-buffered saline (PBS) and incubated with an equilibration buffer before incubation with dUTP-digoxigenin with terminal deoxynucleotidyl transferase (TdT enzyme) in a humidified chamber for 1 h at 37 °C. The reaction was stopped in stop wash buffer and tissue sections were washed in PBS before incubation with an anti-digoxigenin antibody that is conjugated to a peroxidase reporter molecule in a humidified chamber for 30 min. This antibody conjugate binds to the fragmented DNA strands that were labelled during incubation with TdT enzyme and reacts with a peroxidase substrate to create the orange-brown staining indicative of apoptosis. After the incubation step with diaminobenzidine (DAB) peroxidase substrate, the slides were washed and counterstained with Mayer's hematoxylin to allow observation of intact nuclei alongside apoptotic nuclei. Slides were then washed and cleared with n-butanol and xylene before applying the coverslip with Permount mounting medium.

Photographs of tissue sections were taken at 400x magnification at three random locations along the surface body wall (SBW), basal body wall (BBW) and mesenteries for a total of nine photographs per section. Example micrographs with pertinent information are presented in this report to demonstrate preliminary results. Due to delays caused by the COVID-19 pandemic, the full quantitative and qualitative analysis of cell death will be completed in future work. Photographs will be examined for the presence and abundance of apoptotic and intact nuclei and a ratio will be calculated via cell counts. To compare cell death information with other signs of histopathology, the corresponding location of each photograph will be located in the tissue section stained with hematoxylin and eosin. Any apparent spatial patterns or relationships with other morphological indications of disease in the cells and tissues will be recorded in a spreadsheet.

2.3.3 Methods development: TUNEL Method for apoptosis on paraffin-embedded coral tissues

To ensure the validity of staining results, multiple protocol trials were examined to determine the most effective strategy for using the TUNEL method to highlight apoptotic cells in paraffin-embedded coral tissues, since it was optimized for use on mammalian tissues. In addition to staining slides according to the manufacturer's instructions for the Apoptag Peroxidase In-Situ Apoptosis Detection Kit, the following aspects of the protocol were tested using:

- The **addition of a blocking step to reduce the amount of non-specific antibody binding** to tissues. After the incubation period with TdT enzyme and Reaction Buffer, a 30-min incubation step with Roche blocking reagent was added before incubation with the anti-digoxigenenin conjugate.

- **Multiple concentrations of proteinase-K**, the digestive enzyme used to expose antigens that are masked by the protein crosslinking that form during fixation, were tested for best results. While this step is necessary for increasing the antibody-epitope binding that labels apoptotic cells, it has been reported that excessive incubation or excessive concentrations of proteinase-K can cleave DNA strands and cause false-positive staining for apoptosis (Garrity et al. 2003). To ensure that this was not occurring, we tested the protocol with a gradient of proteinase-K concentrations on serial sections from the same

tissue sample: 5 µL/mL, 10 µL/mL, 12 µL/mL, 15 µL/mL, and 20 µL/mL (concentration recommended by manufacturer).

- **Numerous incubation times with proteinase-K** were also tested to ensure that the exposure to this digestive enzyme was not causing false positive staining by chemically cleaving DNA strands. The protocol was repeated on serial sections of the same tissue sample with an incubation in 20 µL/mL for a duration of 5 min, 10 min, and 15 min (duration recommended by manufacturer).

- **Alternative antigen-retrieval methods** were also explored to ensure that the amount of positive staining was not related to the method, which would indicate that DNA fragmentation was being caused by the protocol and was not reflective of genuine cellular processes prior to fixation. Instead of the proteinase-K digestive enzyme, which enzymatically breaks the protein cross links that are formed during fixation (called "proteolytic-induced epitope retrieval, or PIER), these links can also be broken by heat (called "heat-induced epitope retrieval, HIER), or through incubation with a detergent. To test these three alternative techniques, serial sections of the same tissue sample were treated with 20 µL/mL of proteinase-K for 15 min at room temperature (PIER method recommended by the manufacturer), treated with 10 mM citrate buffer and heated for three 3-min cycles in a microwave (HIER method) or incubated in 0.5% TRITON X-100 for 10 min at room temperature (detergent method).

- **Alternative counterstains** were explored to reduce the over-staining of coral mucus in the specimens, which obscures the nuclei that are the focus of this protocol. Sections were counterstained with either 0.5% methyl green (free of crystal violet, recommended by manufacturer) or Mayer's hematoxylin for comparison.

3. RESULTS

3.1. Task 1

3.1.2 DNA Extraction

The DNA concentrations of extracted samples ranged from 71.3 ng/ml to >100,000 ng/ml. The average concentration across all samples was 16,770.2 ng/ml (n=50). Extracted DNA from the apparently diseased samples ranged in concentration from 76 ng/ml to 4290 ng/ml with a mean concentration of 1522 ng/ml (n=8). Extracted DNA from the apparently healthy samples ranged in concentration from 71.3 ng/ml to >100,000 ng/ml with a mean concentration of 21258.1 ng/ml (n=34). Extracted DNA from the unaffected areas of apparently diseased samples ranged in concentration from 76.7 ng/ml to 31,900 ng/ml with a mean concentration of 11,524 ng/ml (n=8). PCLI samples had an average concentration of 2,446.5 ng/ml (n=2). MCAV samples had an average concentration of 6853.9 ng/ml (n=15). DLAB samples had an average concentration of 7659.2 ng/ml (n=9). CNAT samples had an average concentration of 19,570.6 ng/ml (n=10). SSID samples had an average concentration of 21,717.5 ng/ml (n=8). OFAV samples had an average concentration of 46,717.5 ng/ml (n=4). PAST samples had an average DNA concentration of 52,780 ng/ml (n=2).

3.1.3 Polymerase Chain Reaction (PCR) Amplification of Bacterial, Archaeal, and Fungal Marker Genes

Twenty-nine of 51 processed and extracted samples (58%) were successfully PCR-amplified using bacterial/archaeal-specific primers. These included 10/10 processed CNAT samples (100%), 2/2 processed PAST samples (100%), 4/8 processed SSID samples (50%), 3/4 processed OFAV samples (75%), 4/9 processed DLAB samples (44%), 1/15 processed MCAV samples (6.6%). No PCLI samples were successfully amplified 0/2 (0%). Twenty-seven of 51 processed and extracted samples (54%) successfully PCR-amplified using fungal-specific primers. These included 10/10 processed CNAT samples (100%), 2/2 processed PAST samples (100%), 7/8 processed SSID samples (87.5%), 3/4 processed OFAV samples (75%), 3/9 processed DLAB samples (33.3%), 2/15 processed MCAV samples (13.3%). No PCLI samples were successfully amplified 0/2 (0%).

3.1.4 Microbiome Composition Based on Sequencing and Bioinformatic Analysis

For 16S rRNA gene amplicons, a total of 4.4 million sequences were retrieved, with an average of 176,697 sequences per sample prior to quality filtering, denoising, merging, and chimera removal. A total of 686,703 sequences, with an average of 27,468 sequences per sample remained after these processes. Preliminary results from principal coordinates analysis (PCoA) based on Bray-Curtis distances revealed that samples collected from Martin County clustered closely together regardless of species (Figure 4). Furthermore, samples secondarily clustered by diseased state, with healthy colonies from all species clustered closer together and unaffected and diseased CNAT and DLAB colonies more dispersed. A preliminary examination of the relative abundance of taxa across samples reveals a high presence (~50%) of unassigned taxa that, upon further inspection with BLASTn, were largely uncultured prokaryote or bacterium clones (Figure 5). Eukaryotic sequences were also present. Further bioinformatic optimization is needed to resolve these issues. The kit blank and PCR negative had relatively few sequences (in the hundreds) but some bacterial taxa were identified. At the class level Gammaproteobacteria, Bacteroidia, Alphaproteobacteria, Planctomycetes, Cyanobacteria and Phycisphaerae were present in all coral samples at decreasing abundances. Clostridia was present in nearly all samples with no discernable pattern between species or health state. Blastocatellia appeared to be relatively more abundant in diseased and unaffected CNAT and one diseased DLAB colony in comparison to healthy colonies of conspecifics and other species.

For ITS gene amplicons, a total of 4.3 million sequences were retrieved, with an average of 152,792 sequences per sample prior to quality filtering, denoising, merging, and chimera removal. A total of 1.4 million sequences, with an average of 49,817 sequences per sample remained after these processes. Preliminary results from principal coordinates analysis (PCoA) based on Bray-Curtis distances revealed that samples clustered primarily based on species and disease state (Figure 6). In particular, samples taken from unaffected and diseased portions of CNAT colonies clustered closely together, indicating that unaffected portions of those colonies had similar, if not almost the same, fungal composition as diseased portions. A preliminary

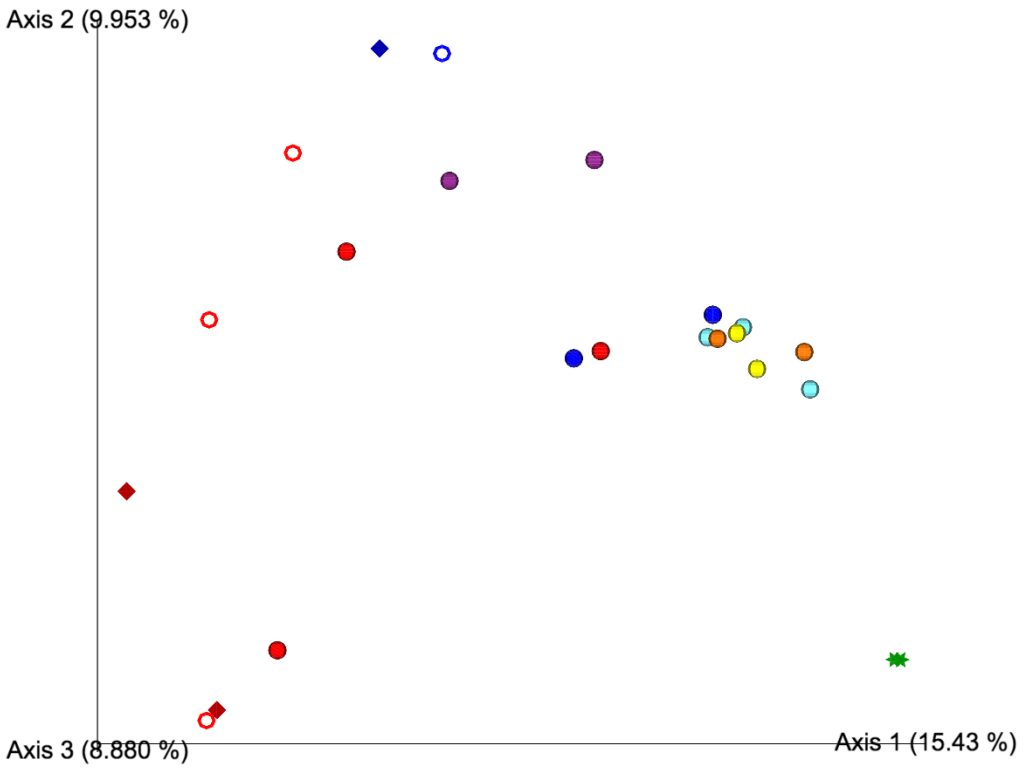

Figure 4: Principal coordinates analysis (PCoA) plot based on Bray-Curtis distances for 16S rRNA gene amplicon sequences. Points that are closer together are more similar in microbial community composition and those that are further apart are more dissimilar. Red points = CNAT, dark blue = DLAB, orange = MCAV, purple = OFAV, yellow = PAST, light blue = SSID, and green = PCR positive. Spheres = healthy, rings = unaffected, diamonds = diseased, stars = PCR positive.

examination of the relative abundance of taxa across samples reveals a high presence of unidentified fungi (Figure 7). A fungus from the *Cortinarius* genus was present in all CNAT samples, but appeared to be relatively more abundant in unaffected and diseased samples, with the exception of one apparently healthy colony. The Agaricomycetes class was comprised ~30% of taxa in two apparently healthy CNAT samples and was in low abundance or absent in all other samples, including unaffected and diseased CNAT.

All raw sequence data from these samples will be publicly available through NCBI's Sequence Read Archive (SRA) database. The 16S rRNA gene amplicon sequences will be made available to the Disease Advisory Committee for inclusion in a meta-analysis being performed by a working group within the Pathogen ID/Microbiome SubTeam.

3.2. Task 2

Initial results from the histoslide examinations showed multiple types of necrosis and degradation within and around the zooxanthellae in apparently healthy, diseased, and unaffected

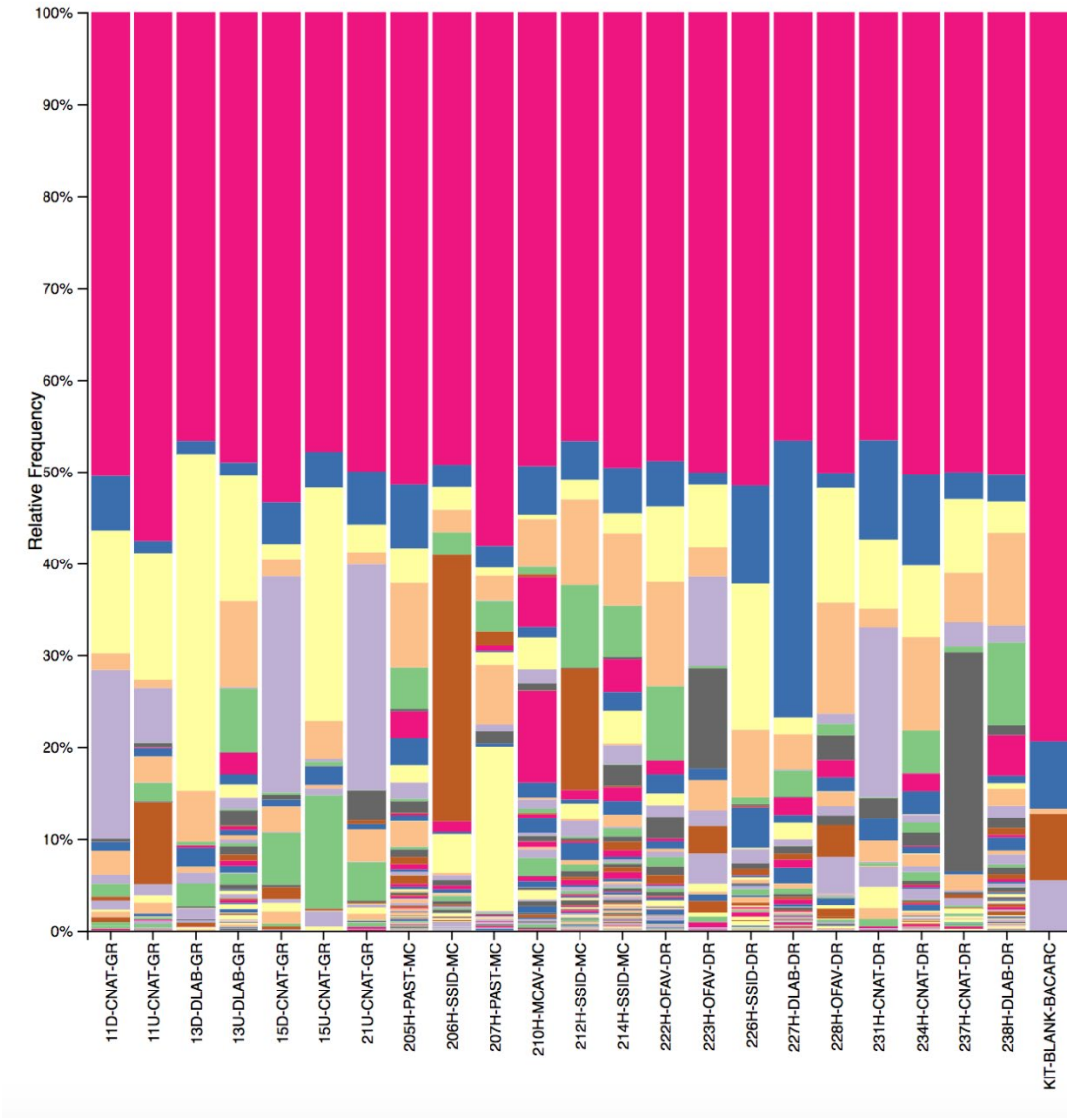

Figure 5: Taxonomic bar plot summary for 16S rRNA gene amplicon sequences (class level). The x-axis contains sample IDs: sample number, health state (H = healthy, U = unaffected, D = diseased), coral species, location collected, gene amplicon). The y-axis is the relative abundance of different taxa in each sample. A kit blank was also included for comparison. Color codes for all groups are on the next page.


Unassigned;__;__
d__Bacteria;p__Proteobacteria;c__Gammaproteobacteria
d__Bacteria;p__Bacteroidota;c__Bacteroidia
d__Bacteria;p__Proteobacteria;c__Alphaproteobacteria
d__Bacteria;p__Halanaerobiaeota;c__Halanaerobiia
d__Bacteria;p__Planctomycetota;c__Planctomycetes
d__Bacteria;p__Desulfobacterota;c__Desulfobacteria
d__Bacteria;p__Firmicutes;c__Bacilli
d__Bacteria;p__Chloroflexi;c__Anaerolineae
d__Bacteria;p__Cyanobacteria;c__Cyanobacteriia
d__Archaea;p__Crenarchaeota;c__Nitrososphaeria
d__Bacteria;p__Firmicutes;c__Clostridia
d__Bacteria;__;__
d__Bacteria;p__Acidobacteriota;c__Blastocatellia
d__Bacteria;p__Planctomycetota;c__Phycisphaerae
d__Bacteria;p__Chloroflexi;c__Chloroflexia
d__Bacteria;p__Chloroflexi;c__Dehalococcoidia
d__Bacteria;p__Acidobacteriota;c__Vicinamibacteria
d__Bacteria;p__Fusobacteriota;c__Fusobacteriia
d__Bacteria;p__Planctomycetota;c__OM190
d__Bacteria;p__Spirochaetota;c__Spirochaetia
d__Bacteria;p__Dadabacteria;c__Dadabacteriia
d__Bacteria;p__Myxococcota;c__Polyangia
d__Bacteria;p__NB1-j;c__NB1-j
d__Bacteria;p__Acidobacteriota;c__Thermoanaerobaculia
d__Bacteria;p__Gemmatimonadota;c__BD2-11_terrestrial_group
d__Bacteria;p__Firmicutes;c__TSAC18
d__Bacteria;p__Firmicutes;c__Dethiobacteria
d__Bacteria;p__Verrucomicrobiota;c__Verrucomicrobiae
d__Bacteria;p__Verrucomicrobiota;c__Chlamydiae
d__Bacteria;p__Chloroflexi;c__JG30-KF-CM66
d__Bacteria;p__Planctomycetota;c__Pla3_lineage
d__Bacteria;p__Entotheonellaeota;c__Entotheonellia
d__Bacteria;p__SAR324_clade(Marine_group_B);c__SAR324_clade(M
d__Bacteria;p__Actinobacteriota;c__Thermoleophilia
d__Bacteria;p__Bdellovibrionota;c__Bdellovibrionia
d__Bacteria;p__Chloroflexi;c__TK17
d__Bacteria;p__PAUC34f;c__PAUC34f
d__Bacteria;p__Nitrospirota;c__Nitrospiria
d__Eukaryota;__;__
d__Bacteria;p__Acidobacteriota;c__Acidobacteriae
d__Bacteria;p__Bacteroidota;c__Rhodothermia
d__Bacteria;p__Patescibacteria;c__Gracilibacteria
d__Bacteria;p__Latescibacterota;c__Latescibacterota
d__Bacteria;p__Planctomycetota;c__vadinHA49
d__Bacteria;p__Firmicutes;c__Desulfotomaculia
d__Bacteria;p__Acidobacteriota;c__Subgroup_21
d__Bacteria;p__Desulfobacterota;c__Desulfobulbia
d__Bacteria;p__Chloroflexi;c__KD4-96
d__Bacteria;p__Actinobacteriota;c__Actinobacteria
d__Bacteria;p__Poribacteria;c__Poribacteria
d__Bacteria;p__Planctomycetota;c__Pla4_lineage
d__Bacteria;p__Deinococcota;c__Deinococci
d__Bacteria;p__Proteobacteria;__
d__Bacteria;p__Myxococcota;c__bacteriap25
d__Bacteria;p__Spirochaetota;c__Leptospirae
d__Bacteria;p__Firmicutes;c__Moorellia
d__Bacteria;p__Chloroflexi;c__TK10
d__Bacteria;p__Desulfobacterota;c__uncultured
d__Bacteria;p__Nitrospinota;c__Nitrospinia
d__Eukaryota;p__Dinoflagellata;c__Dinophyceae
d__Bacteria;p__Bacteroidota;c__Ignavibacteria
d__Bacteria;p__Chloroflexi;c__TK30
d__Bacteria;p__Gemmatimonadota;c__PAUC43f_marine_benthic_gro
d__Archaea;p__Thermoplasmatota;c__Thermoplasmata
d__Bacteria;p__Acidobacteriota;__
d__Bacteria;p__Desulfobacterota;c__Desulfuromonadia
d__Bacteria;p__Myxococcota;c__Myxococcia
d__Bacteria;p__Desulfobacterota;c__Desulfarculia
d__Bacteria;p__Margulisbacteria;c__Margulisbacteria
d__Bacteria;p__Desulfobacterota;c__Desulfovibrionia
d__Bacteria;p__Acidobacteriota;c__Subgroup_22
d__Bacteria;p__Bacteroidota;c__Kapabacteria
d__Bacteria;p__Calditrichota;c__Calditrichia
d__Bacteria;p__Campilobacterota;c__Campylobacteria
d__Bacteria;p__Patescibacteria;c__ABY1
d__Bacteria;p__Nitrospinota;c__P9X2b3D02
d__Bacteria;p__Verrucomicrobiota;c__Omnitrophia
d__Bacteria;p__Actinobacteriota;c__Acidimicrobiia
d__Bacteria;p__Planctomycetota;__
d__Bacteria;p__Acetothermia;c__Acetothermiia
d__Bacteria;p__Acidobacteriota;c__Subgroup_26
d__Bacteria;p__Cyanobacteria;c__Vampirivibrionia
d__Archaea;p__Nanoarchaeota;c__Nanoarchaeia
d__Bacteria;p__AncK6;c__AncK6
d__Bacteria;p__Acidobacteriota;c__Subgroup_11
d__Bacteria;p__Bdellovibrionota;c__Oligoflexia
d__Bacteria;p__Hydrogenedentes;c__Hydrogenedentia
d__Bacteria;p__Planctomycetota;c__BD7-11
d__Bacteria;p__Dependentiae;c__Babeliae
d__Bacteria;p__Firmicutes;__
d__Bacteria;p__Verrucomicrobiota;c__Lentisphaeria
d__Bacteria;p__Acidobacteriota;c__AT-s3-28
d__Bacteria;p__Myxococcota;__
d__Bacteria;p__Spirochaetota;c__V2072-189E03
d__Bacteria;p__Verrucomicrobiota;c__Kiritimatiellae
d__Bacteria;p__Firmicutes;c__Desulfitobacteriia
d__Eukaryota;p__Chlorophyta;__
d__Bacteria;p__Acidobacteriota;c__Aminicenantia
d__Bacteria;p__Latescibacterota;c__Latescibacteria
d__Bacteria;p__Chloroflexi;__
d__Bacteria;p__Patescibacteria;c__Parcubacteria
d__Bacteria;p__WPS-2;c__WPS-2
d__Bacteria;p__Gemmatimonadota;c__Gemmatimonadetes
d__Bacteria;p__Schekmanbacteria;c__Schekmanbacteria
d__Bacteria;p__MBNT15;c__MBNT15
d__Bacteria;p__Bacteroidota;c__Kryptonia
d__Bacteria;p__Modulibacteria;c__Moduliflexia
d__Bacteria;p__NKB15;c__NKB15
d__Bacteria;p__Acidobacteriota;c__Holophagae
d__Bacteria;p__WS2;c__WS2
d__Bacteria;p__Sumerlaeota;c__Sumerlaeia
d__Bacteria;p__Planctomycetota;c__Brocadiae
d__Archaea;p__Asgardarchaeota;c__Odinarchaeia
d__Bacteria;p__Planctomycetota;c__028H05-P-BN-P5
d__Eukaryota;p__Cnidaria;c__Anthozoa
d__Bacteria;p__Synergistota;c__Synergistia
d__Bacteria;p__Marinimicrobia_(SAR406_clade);c__Marinimicrobia_(S
d__Bacteria;p__Armatimonadota;c__Fimbriimonadia
d__Bacteria;p__Desulfobacterota;c__Desulfomonilia
d__Bacteria;p__Chloroflexi;c__N9D0
d__Bacteria;p__Sva0485;c__Sva0485
d__Bacteria;p__Elusimicrobiota;c__Lineage_IIb
d__Eukaryota;p__Chlorophyta;c__Ulvophyceae
d__Bacteria;p__Bacteroidota;c__Chlorobia
d__Eukaryota;p__MAST-3;c__MAST-3I
d__Eukaryota;p__Labyrinthulomycetes;c__Labyrinthulomycetes
d__Archaea;p__Aenigmarchaeota;c__Aenigmarchaeia
d__Bacteria;p__RCP2-54;c__RCP2-54
d__Archaea;p__Aenigmarchaeota;c__Deep_Sea_Euryarchaeotic_Grou
d__Archaea;__;__
d__Bacteria;p__Desulfobacterota;c__Syntrophia
d__Bacteria;p__Zixibacteria;c__Zixibacteria
d__Bacteria;p__WOR-1;c__WOR-1
d__Bacteria;p__Fibrobacterota;c__Fibrobacteria
d__Bacteria;p__Elusimicrobiota;c__Lineage_IIc
d__Bacteria;p__Elusimicrobiota;c__Elusimicrobia
d__Bacteria;p__LCP-89;c__LCP-89
d__Archaea;p__Asgardarchaeota;c__Lokiarchaeia
d__Bacteria;p__Spirochaetota;c__Brachyspirae
d__Eukaryota;p__Apicomplexa;c__Conoidasida
d__Bacteria;p__Spirochaetota;__
d__Bacteria;p__Patescibacteria;c__Microgenomatia
d__Bacteria;p__Deferrisomatota;c__Defferrisomatia
d__Bacteria;p__Cyanobacteria;c__Sericytochromatia
d__Bacteria;p__Bacteroidota;__
d__Archaea;p__Crenarchaeota;c__Bathyarchaeia
d__Eukaryota;p__Phragmoplastophyta;c__Embryophyta
d__Eukaryota;p__Cnidaria;__
d__Bacteria;p__Actinobacteriota;__

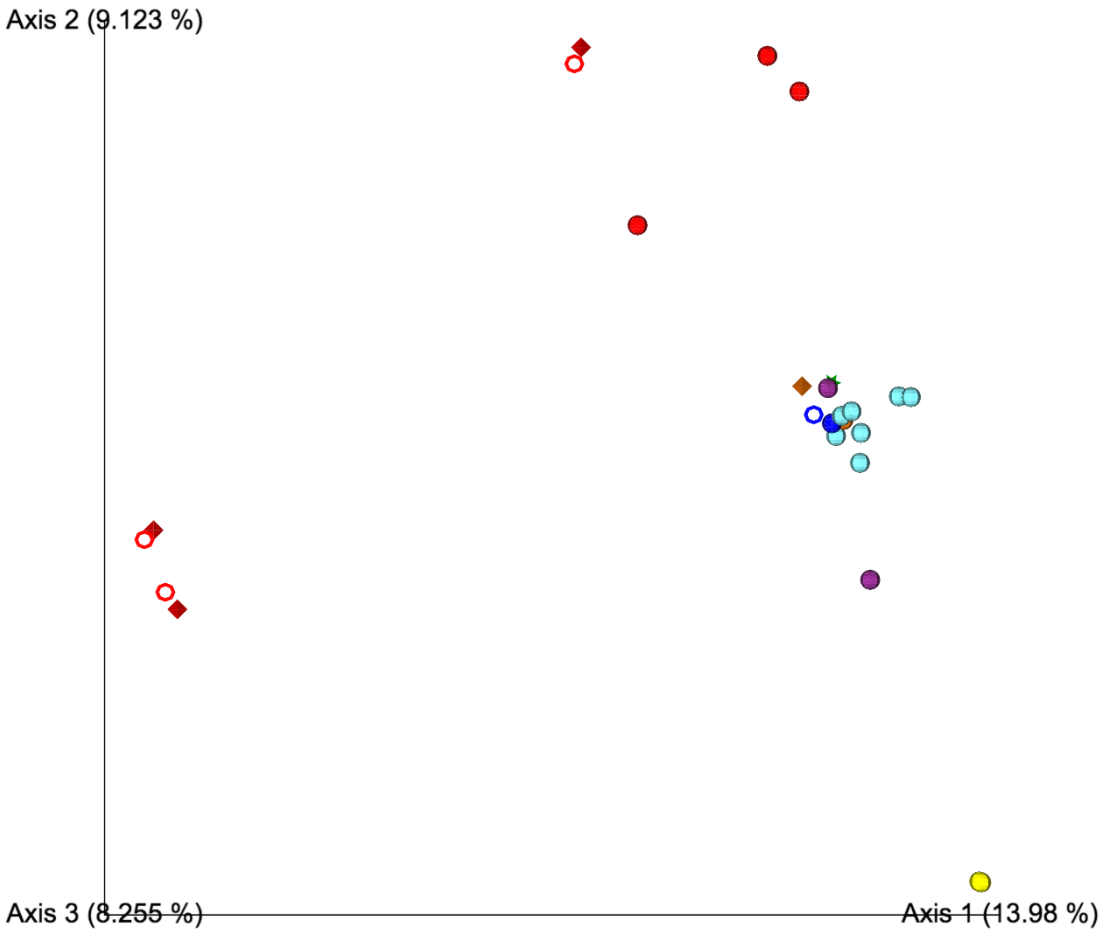

Figure 6: Principal coordinates analysis (PCoA) plot based on Bray-Curtis distances for ITS gene amplicon sequences. Points that are closer together are more similar in fungal community composition and those that are further apart are more dissimilar. Red points = CNAT, dark blue = DLAB, orange = MCAV, purple = OFAV, yellow = PAST, light blue = SSID, and green = PCR positive. Spheres = healthy, rings = unaffected, diamonds = diseased, stars = PCR positive.

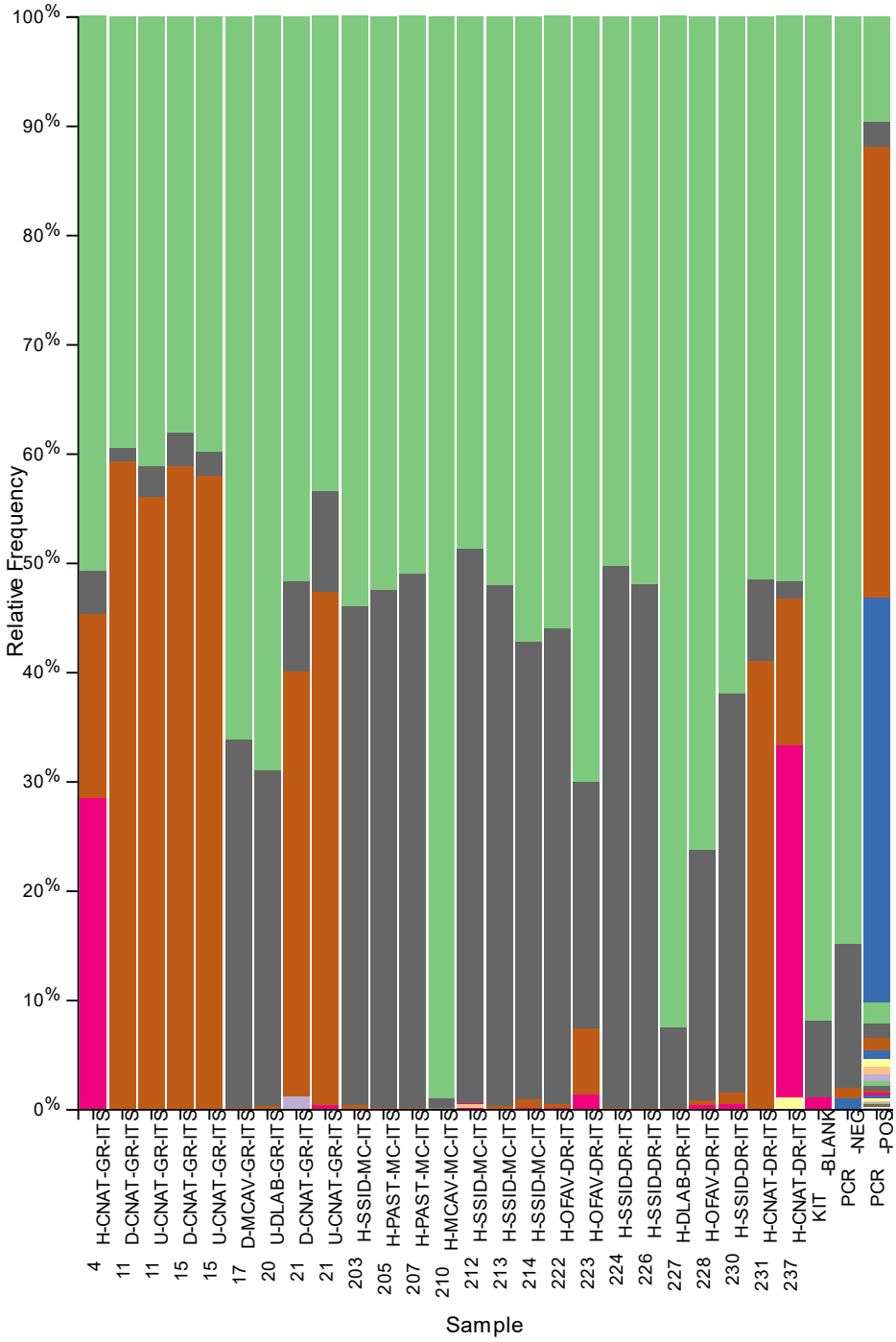

Figure 7: Taxonomic bar plot summary for ITS gene amplicon sequences (species level). The x-axis contains sample IDs: sample number, health state (H = healthy, U = unaffected, D = diseased), coral species, location collected, gene amplicon). The y-axis is the relative abundance of different taxa in each sample. A kit blank as well as PCR positive and negative controls were also included for comparison. Color codes for all groups are on the next page.

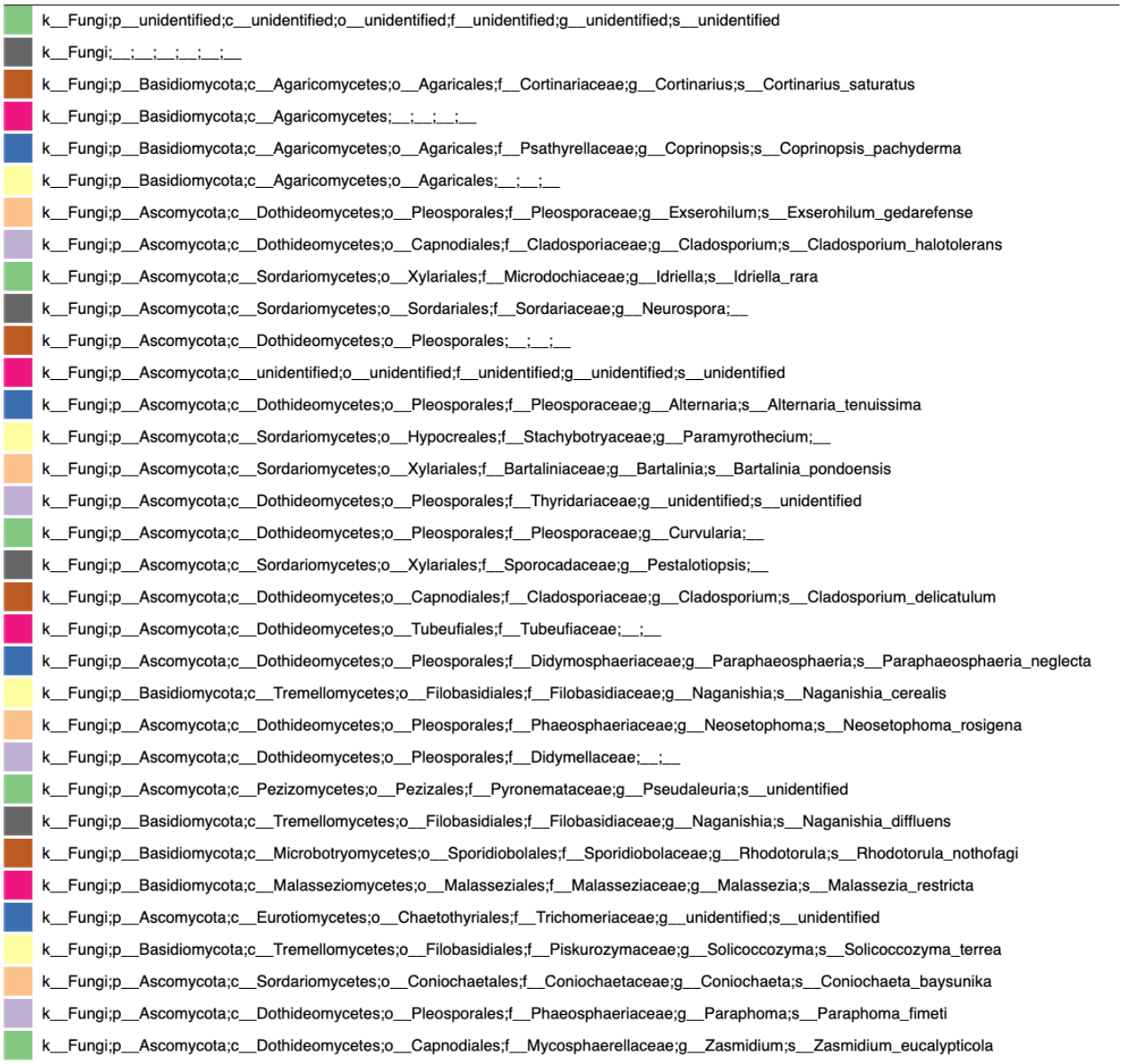

tissue samples from all four species of coral examined. Few cases of 'healthy' tissue were observed.

3.2.1 Necrosis

Liquefactive necrosis (LN) was the most common type of cell death observed across all species (Figure 8). The necrotic tissue within the SBW gastrodermis appeared as fluid-like spaces with few to no zooxanthellae. These lesions were usually restricted to the gastrodermal tissue with the mesoglea and epidermis intact. In some cases, the gastrodermis of the SBW detached from mesoglea either partially or completely. Areas of LN were isolated with surrounding tissue showing signs of degradation, including vacuolation and lysing, with the algal cells appearing pale as staining quality decreased and the cell wall disintegrated (ghosting). Pyknosis was also

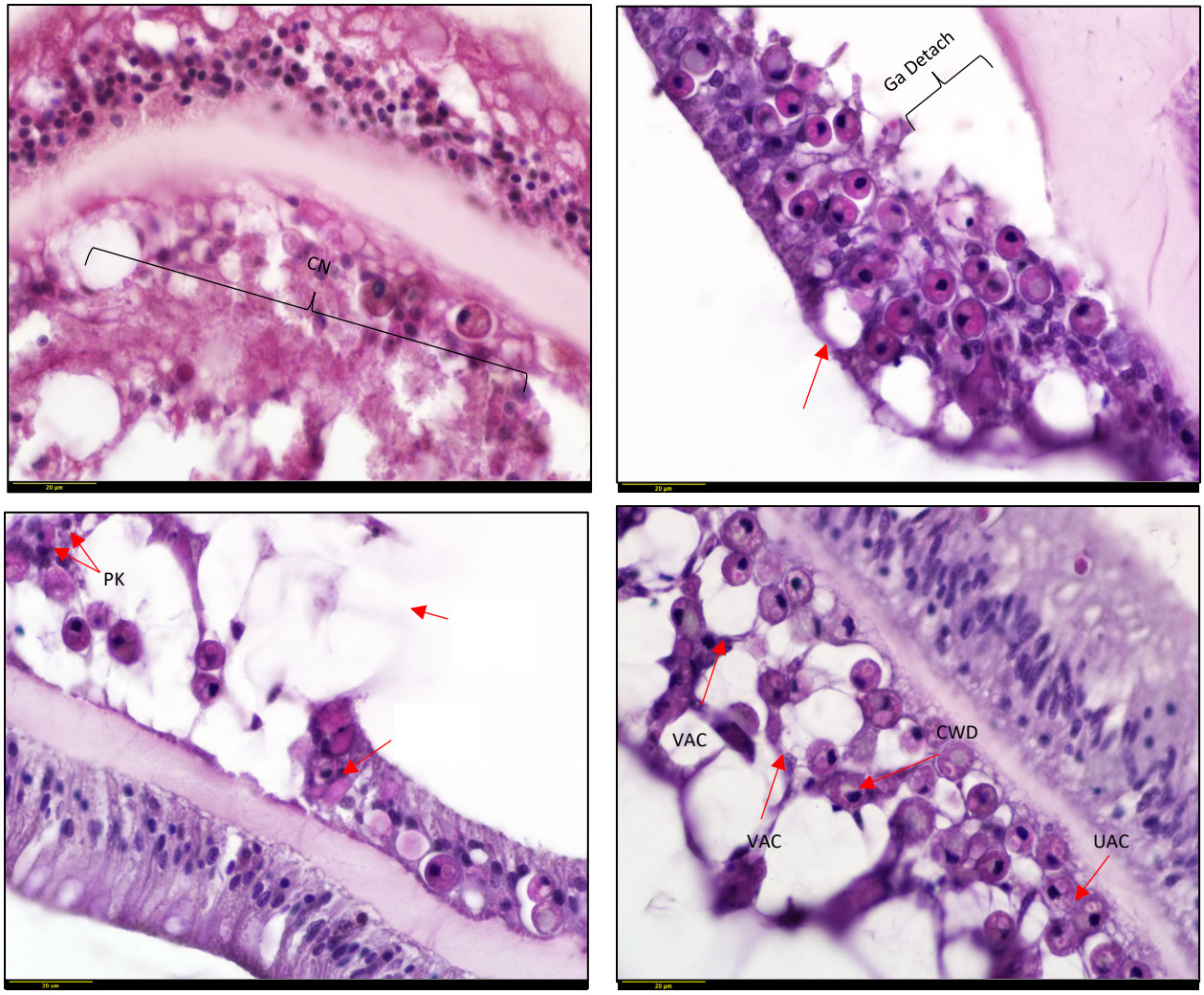

Figure 8: Epithelial damage. Upper left: MCAV 114D, coagulative necrosis (CN), Upper right: MCAV 102D gastrodermal detachment (Ga Detach) from mesoglea with vacuolation (VAC), Bottom left: MCAV 103D Liquefactive necrosis (LN) with pyknotic (PK) algal cells, Bottom right: MCAV 104U Vacuolation within gastrodermis with uric acid crystals (UAC) and cell wall disintegration (CWD) in algal cells.

observed in the surrounding tissues. LN was seen in diseased, unaffected, and apparently healthy coral samples (Table 4).

Besides being observed in areas near LN, pyknosis was common in tissue that was considered degraded, most frequently in areas of vacuolation. Coagulative necrosis was only seen in a few cases, most noticeably in MCAV 104HD, which also had abundant zooxanthellae containing uric acid crystals (Figure 8).

3.2.2 Degradation

Degradation of the dinoflagellate cells was scored in six different ways. Of the 54 slides analyzed, only vacuolation, cell wall disintegration (ghosting), swelling, and uric acid crystals

Table 4: Number of samples affected by the different types of necrosis in FWRI 2016 histoslides. H = healthy, D = diseased, U = unaffected.

Lesion Type →	Lique-factive	Lique-factive	Lique-factive	Coagu-lative	Coagu-lative	Coagu-lative	Pyk-notic	Pyk-notic	Pyk-notic
Species	H (n =)	D (n =)	U (n =)	H (n =)	D (n =)	U (n =)	H (n =)	D (n =)	U (n =)
DLAB	0	0	2	0	0	0	0	0	1
MCAV	4	11	7	2	1	0	2	11	7
SSID	1	2	3	0	0	0	0	2	0
OFAV		2	3		0	0		1	1
Total	**5**	**15**	**15**	**2**	**1**	**0**	**2**	**14**	**9**

were seen (Table 5). Gold-brown zooxanthellae or the presence of melanin was not evident in any of the photomicrographs examined.

Vacuolation was the most common cellular change present, in 49 of the 54 histoslides analyzed. The severity varied, although it was not more frequent in any one species or condition type. It was more pronounced in the algal cells in areas that also showed signs of necrosis or other types of symbiont degradation, such as swelling or ghosting.

Cell wall disintegration (ghosting) was seen in the gastrodermal dinoflagellates of 43 of the 54 histoslides. It was most frequent in areas where the gastrodermis was beginning to detach from the mesoglea and in areas where LN was present. Unlike vacuolation, it was not seen in tissue that looked otherwise healthy but rather in areas already showing other signs of degradation.

Swelling of algal cells was seen in 19 of the 54 histoslides. It was only present in areas that also had vacuolation. The severity of the swelling of the individual zooxanthellae appeared to correspond with the severity of the vacuolation of the space it inhabited.

Uric acid crystals (Clode et al. 2009) were seen rarely, in only 5 of the 54 histoslides. Because they are contained within the zooxanthellae, their presence made it difficult to produce a focused photomicrograph.

3.2.3 Dinoflagellate Counts and Gastrodermal Thickness

Of the 54 slides examined, dinoflagellate counts were completed on 22, including 14 MCAV samples and 7 SSID samples. The calculated averages obtained per 50-µm sections of gastrodermis, percent cells dividing, gastrodermal thickness, and gastrodermal length for those slides are shown in Table 6.

Table 5: Signs of symbiont degradation in FWRI 2016 histoslides. (H) apparently healthy, (D) diseased, (U) unaffected. V = vacuolation, SZ = swollen zooxanthellae, CW = cell wall disintegration and lysing, UA = uric acid crystals in zooxanthellae

Lesion Type →	**V**	**V**	**V**	**SW**	**SW**	**SW**	**CW**	**CW**	**CW**	**UA**	**UA**	**UA**
Species	**H n =**	**D n=**	**U n=**	**H n=**	**D n=**	**U n=**	**H n=**	**D n=**	**U n=**	**H n=**	**D n=**	**U n=**
DLAB H (n=1) D (n=1) U (n=2)	1	1	2	1	1	0	1	1	2	0	0	0
MCAV H (n=6) D (n=14) U (n=12)	3	14	12	1	9	3	3	12	10	0	3	1
SSID H (n=1) D (n=5) U (n=3)	1	4	5	0	2	1	0	4	4	0	0	1
OFAV H (n=1) D (n=2) U (n=3)	1	2	2	0	0	1	1	2	3	0	0	0
Total n=54	6	21	21	2	12	5	5	19	19	0	3	2

Table 6: Zooxanthellae average counts, percent (%) dividing, and average gastrodermal thickness were measured using the averages of each 50-µm section. Average gastrodermal length was calculated by averaging the widest length of the gastrodermis in each photomicrograph.

Species	**Sample Type**	**Zooxanthellae Average Counts/50 µm**	**Zooxanthellae % Dividing**	**Average Gastrodermal Thickness (µm)**	**Average Gastrodermal Length (µm)**
MCAV	H (n=0)			Total Average	Total Average
MCAV	D (n=11)	15	1.2	36.94	142.25
MCAV	U (n=3)	14	2.4		
SSID	H (n=1)	12	1.1	Total Average	Total Average
SSID	D (n=3)	10	4.1	28.93	129.57
SSID	U (n=3)	13	1.6		

3.3. Task 3

3.3.1. Protocol Optimization

The manufacturer's protocol for the Apoptag Peroxidase In Situ Apoptosis Detection Kit is suitable for use on coral tissues with a few changes recommended for more accurate staining (Table 7). To reduce background staining of coral tissues and mucus, adding the additional blocking step between incubation with the TdT enzyme and the antibody conjugate is necessary. The comparison of results from varying the concentration of proteinase-K revealed that the amount (20 µL/mL) given in the instructions was not substantially different from those obtained with lower concentrations. Therefore, using the original concentration in the procedure was not thought to cause false-positive staining through chemically induced DNA fragmentation (Figure 9). Likewise, the recommended duration of proteinase-K exposure (15 min at room temperature) did not produce more positive staining than incubations of shorter durations, indicating that this step also did not create false-positive staining (Figure 10). The proteolytic-induced epitope retrieval method with proteinase-K was found to be the most effective method of exposing antigens, compared to the heat-induced epitope retrieval method (10mM citrate buffer, three 3-min cycles in microwave) and detergent method (0.5% TRITON X-100 for 10 min at room temperature), which both damaged tissues and did not facilitate high resolution staining of nuclei (Figure 11). For coral tissues, the progressive counterstain of Mayer's hematoxylin is more effective for staining only intact nuclei with minimal background staining, whereas the manufacturer-recommended counterstain of 0.5% methyl green was found to bind heavily to coral mucus and obscure cellular morphology from view (Figure 10).

3.3.2: Evidence for apoptosis in SCTLD pathology

In total, twelve samples were fully processed for immunohistochemical analysis of apoptosis and all samples were processed for histopathological examination (Table 8). Tissues from all tested samples displayed cells undergoing apoptosis, including diseased, unaffected, and healthy tissues (Figure 12). Apoptosis also appeared to be present in all tissue layers (epidermis, gastrodermis, calicodermis, and mesenteries), and while preliminary results indicated that the highest abundance of apoptotic nuclei occurred in the basal body wall (BBW), more analysis is needed to confirm this observation (Figure 13). While apoptosis did appear to be abundant in areas of tissue rupture, necrosis, and abnormal zooxanthellae (Figure 14), which have all been noted to be signature components of SCTLD histopathology (Landsberg et al. manuscript in review), further analysis is needed to determine whether (1) apoptosis consistently coincides with these pathologies and (2) whether apoptosis appears to precede or follow their occurrence. Further analysis is also needed to discern any spatial differences within and between tissue layers, as well as any differences between species.

Table 7: Results from methods development trials to optimize the TUNEL method protocol for use on paraffin-embedded coral tissues

Protocol Step	Purpose	Treatments	Best Results	Observations
Addition of Blocking Buffer Step	Reduce background staining of coral mucus and tissues	A) Addition of incubation step with Roche blocking reagent between exposure to TdT enzyme and antibody conjugate, B) Without exposure to blocking reagent*	A) Addition of Blocking Buffer	An additional blocking step reduced the background staining of DAB peroxidase substrate on cytoplasm on mucus, and is recommended particularly for mucus-heavy species
Concentration of proteinase-K	Reduce potential for false positive staining by chemically-induced DAN fragmentation	A) 5 µL/mL, B) 10 µL/mL, C) 12 µL/mL, D) 15 µL/mL, E) 20 µL/mL*	E) 20 µL/mL*	There was no discernable pattern of increasing staining with an increasing gradient of concentration. 20 µL/mL was chosen to align with manufacturer's instructions, though lesser concentrations are acceptable to reduce chemical cost.
Incubation time with proteinase-K	Reduce potential for false positive staining by chemically-induced DAN fragmentation	A) 5 min, B) 10 min, C) 15 min*	C) 15 min*	There was no discernable pattern of increasing staining with an increasing incubation duration. 15 min was chosen to align with manufacturer's instructions, though shorter durations are acceptable to reduce overall protocol time.
Antigen retrieval method	Reduce potential for false positive staining by chemically-induced DAN fragmentation	A) 20 µL/mL proteinase K 15 min* B) 10 mM citrate buffer heated for three 3-min cycles in microwave C) 0.5% TRITON X-100 for 10 min	A) incubation with 20 µL/mL proteinase K for 15 min at room temperature	Exposure to the digestive enzyme proteinase-K resulted in the best resolution of both apoptotic and intact nuclei. The heated method with citrate buffer was damaging to tissue and did not allow for strong staining. The detergent method with 0.5% TRITON X-100 also did not produce intense or refined staining.
Counterstain	Reduce background staining of coral mucus and tissues	A) 0.5% Methyl Green* B) Mayer's Hematoxylin	B) Mayer's Hematoxylin	0.5% Methyl green heavily stained coral mucus and obscured nuclei. Mayer's hematoxylin resulted in sharp staining of intact nuclei with very little-to-no background staining of coral tissues and mucus.

*Treatment recommended by manufacturer

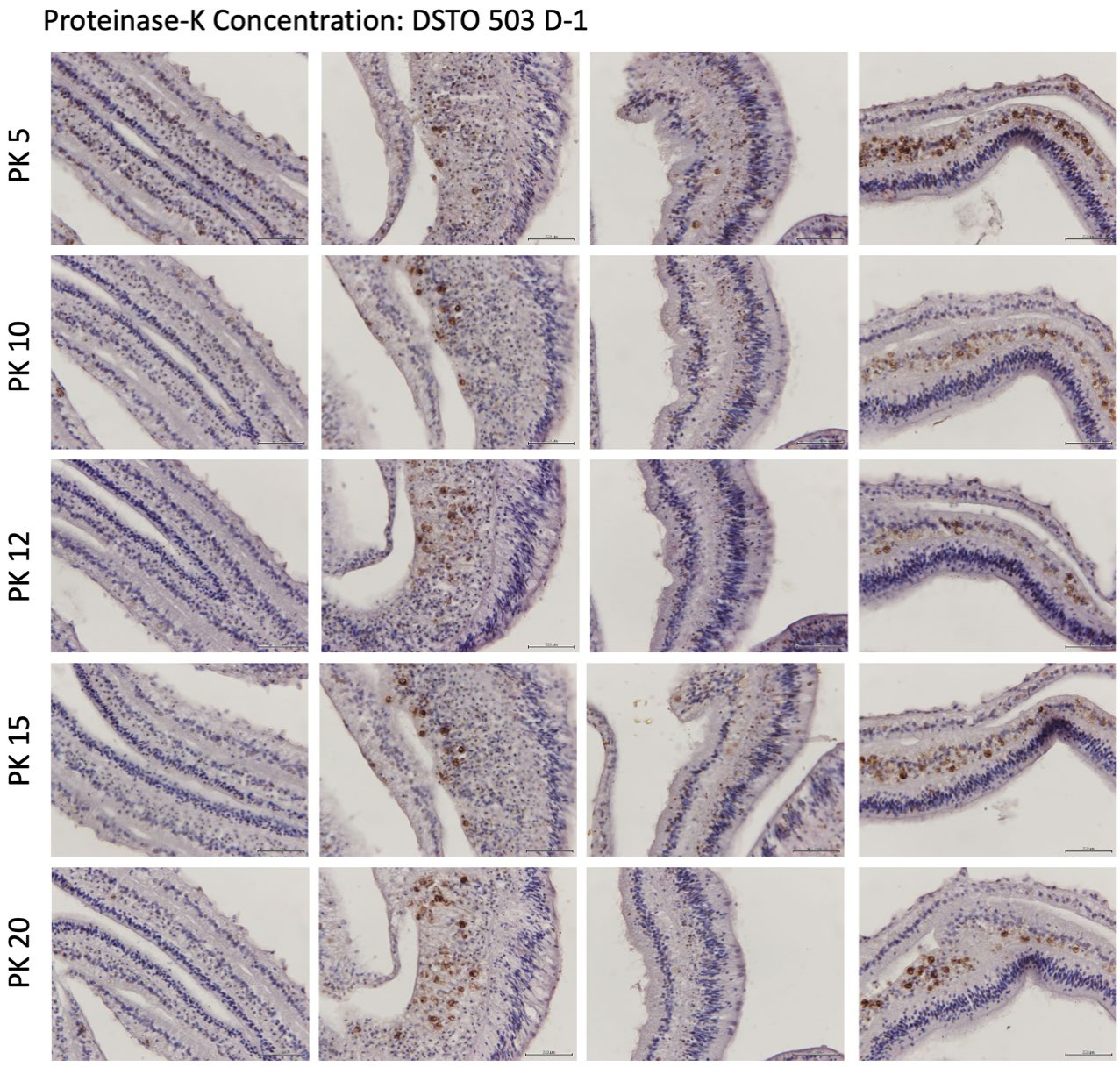

Figure 9: Apoptotic (stained orange-brown) and intact (stained blue) nuclei in the active SCTLD lesion of *Dichoceonia stokesii* incubated in various concentrations of proteinase-K. PK 5 = 5 µl/mL. PK 10 = 10 µl/mL, PK 12 = 12 µl/mL, PK 15 = 15 µl/mL, PK 20 µl/mL. No substantial difference between the number of apoptotic cells in each treatment was observed, variations in staining between treatments is attributed to small differences between the sections as they were taken from the tissue block.

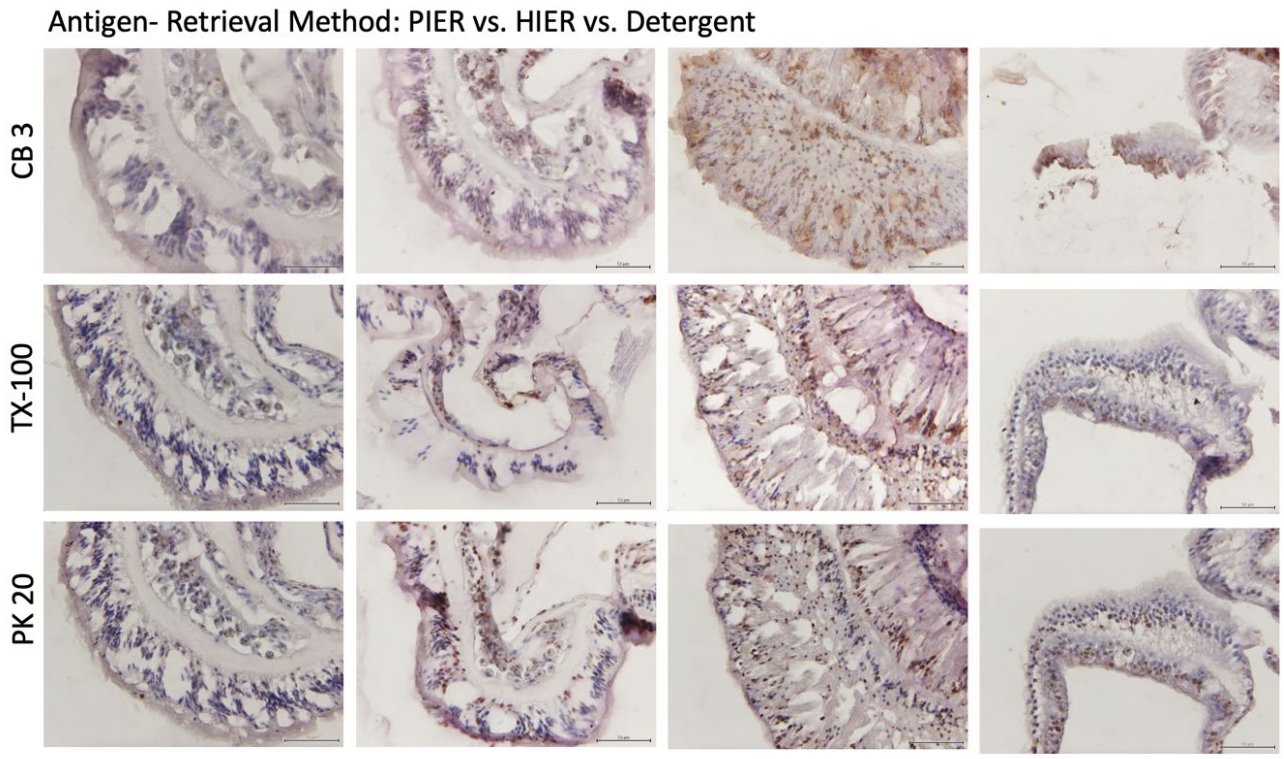

Figure 10: Comparison of staining quality using different epitope-retrieval methods in TUNEL method protocol on diseased tissues of *Pseudodiploria strigosa*. CB 3 = 10 mM citrate buffer, heated for three 3-min cycles in a microwave; TX-100 = 0.5% TRITON X-100 for 10 min at room temperature; PK 20 = 20 µl/mL proteinase-K for 15 min at room temperature. Orange-brown staining indicates apoptotic nuclei, blue staining indicates intact nuclei. Specimens treated with proteinase-K (PK 20) showed best staining results with highly refined nuclei and strong specific staining. The heated treatment in citrate buffer (CB 3) appeared to damage tissues, the detergent treatment with Triton X-100 (TX-100) displayed lower resolution and intensity of staining.

4. DISCUSSION AND RECOMMENDATIONS

4.1. Task 1

DNA extraction data indicate that chemicals may be present in MCAV corals that inhibit the nucleic acid extraction process, resulting in low DNA concentrations. Future work will involve optimizing the DNA extraction process for MCAV and other species through the addition of lysozyme or proteinase K to samples prior to extraction. **Preliminary results revealed patterns bacterial and fungal community composition based on host coral species and disease state, but especially in fungal communities.** Additional samples will be processed and analyzed to provide replicates for more in-depth statistical analysis. Further optimization of the bioinformatic pipeline will be conducted to resolve unassigned and kingdom-assigned reads for both bacterial and fungal datasets. Differentially abundant taxa will be identified in different disease states in more samples. Additional analyses will be conducted on metagenomic sequences to examine functional potential of the coral microbiome in different disease states.

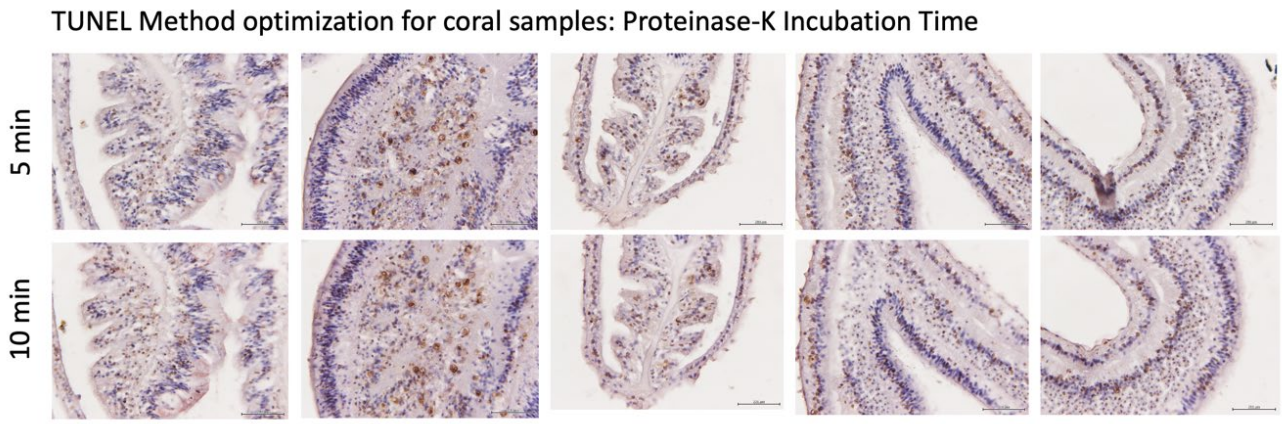

Figure 11: Comparison of positive-staining nuclei that result from 5- and 10-minute incubation times in proteinase-K during TUNEL method protocol on diseased tissues of *Dichocoenia stokesii*. No substantial difference between the number of apoptotic cells in each treatment was observed, variations in staining between treatments is attributed to small differences between the sections as they were taken from the tissue block.

Table 8: Processing status of Task 3 tissue core samples showing the number of slides stained with Apoptag or hematoxylin and eosin (H&E) of the total samples acquired. Diseased samples: 7 Apoptag, 12 H&E total; unaffected: 4 Apoptag, 8 H&E total; apparently healthy: 1 Apoptag, 11 H&E total.

Species	Processing status	Diseased	Diseased	Unaf-fected	Unaf-fected	Apparently Healthy	Apparently Healthy
		Stained	Total	Stained	Total	Stained	Total
PSTR	Apoptag	4	6	1	2	1	3
PSTR	H&E	6	6	2	2	3	3
MCAV	Apoptag	0	2	0	2	0	5
MCAV	H&E	2	2	2	2	2	5
OFAV	Apoptag	0	1	0	1	0	1
OFAV	H&E	0	1	0	1	0	1
DSTO	Apoptag	1	1	1	1		
DSTO	H&E	1	1	1	1		
CNAT	Apoptag	1	1	1	1		
CNAT	H&E	1	1	1	1		
OANN	Apoptag	1	1	1	1		
OANN	H&E	1	1	1	1		

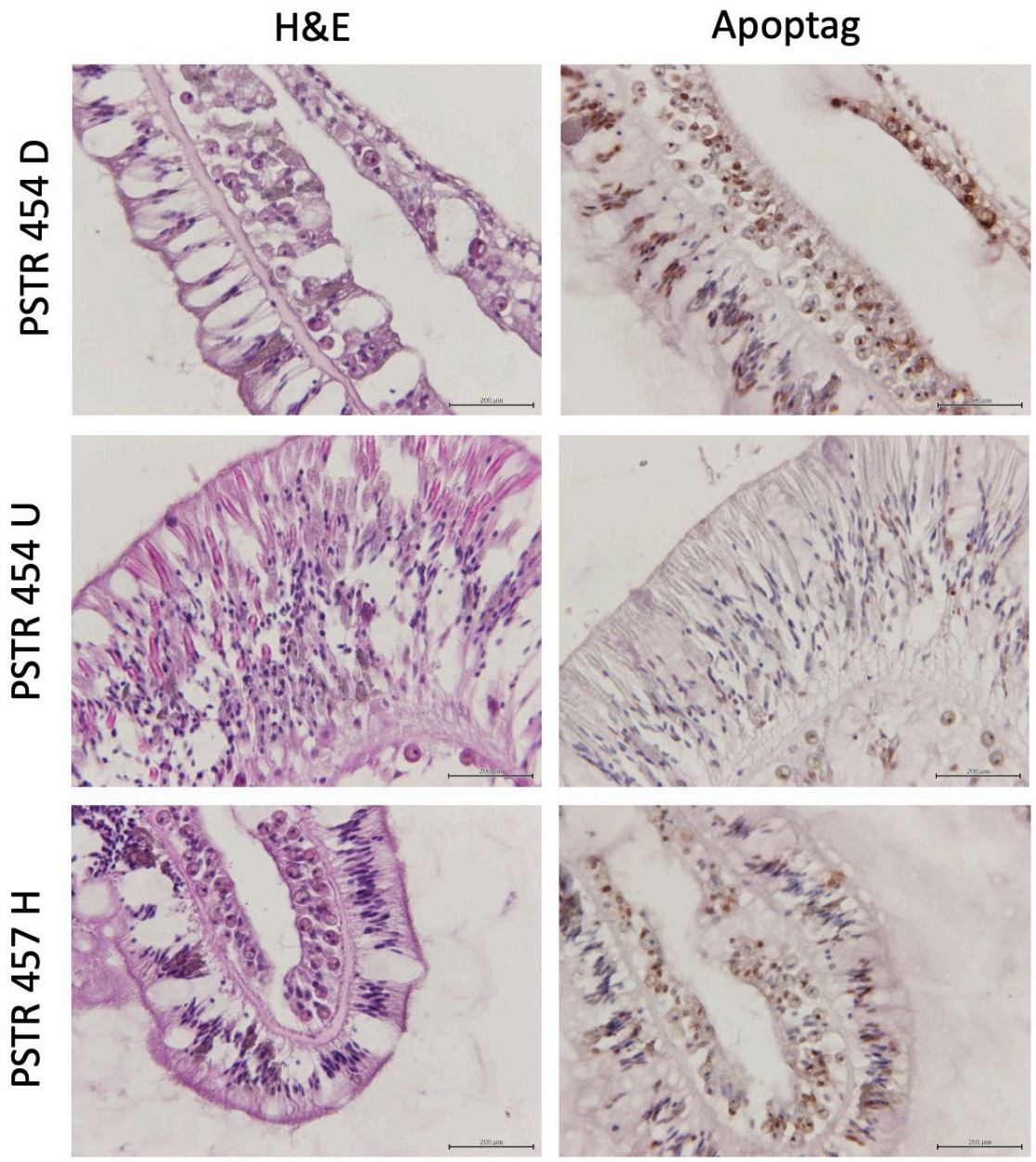

Figure 12: Comparison of tissue sections of healthy, diseased, and unaffected tissues of *Pseudodiploria strigosa* stained with either hematoxylin and eosin or Apoptag Peroxidase In Situ Apoptosis Detection Kit. PSTR 454 D = Diseased, PSTR 454 U = Unaffected, PSTR 457 H = Apparently healthy. In photomicrographs stained with Apoptag, orange-brown staining indicates apoptotic nuclei, blue staining indicates intact nuclei. Apoptotic nuclei are present in all tissue types, diseased, unaffected, and apparently healthy.

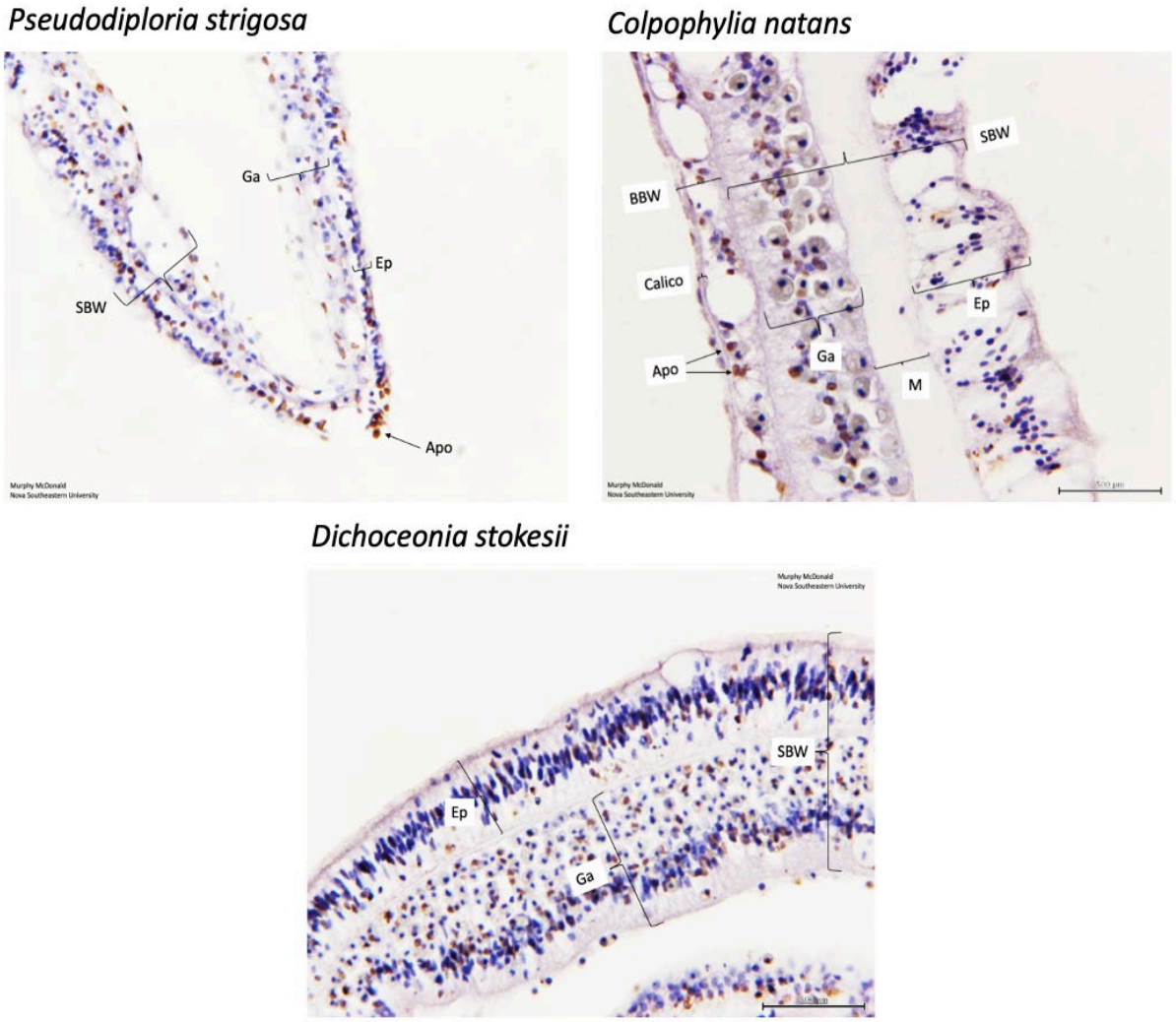

Figure 13: Micrographs of diseased tissues of *Pseudodiploria strigosa*, *Colpophyllia natans*, and *Dichoceonia stokesii* stained with Apoptag Peroxidase In Situ Apoptosis Detection Kit. Orange-brown staining indicates apoptotic nuclei, blue staining indicates intact nuclei. Ga = Gastrodermis, SBW = surface body wall, Ep = epidermis, BBW = basal body wall, Calico = calicodermis, M = mesoglea. Apoptosis was detected in all species tested and all tissue layers.

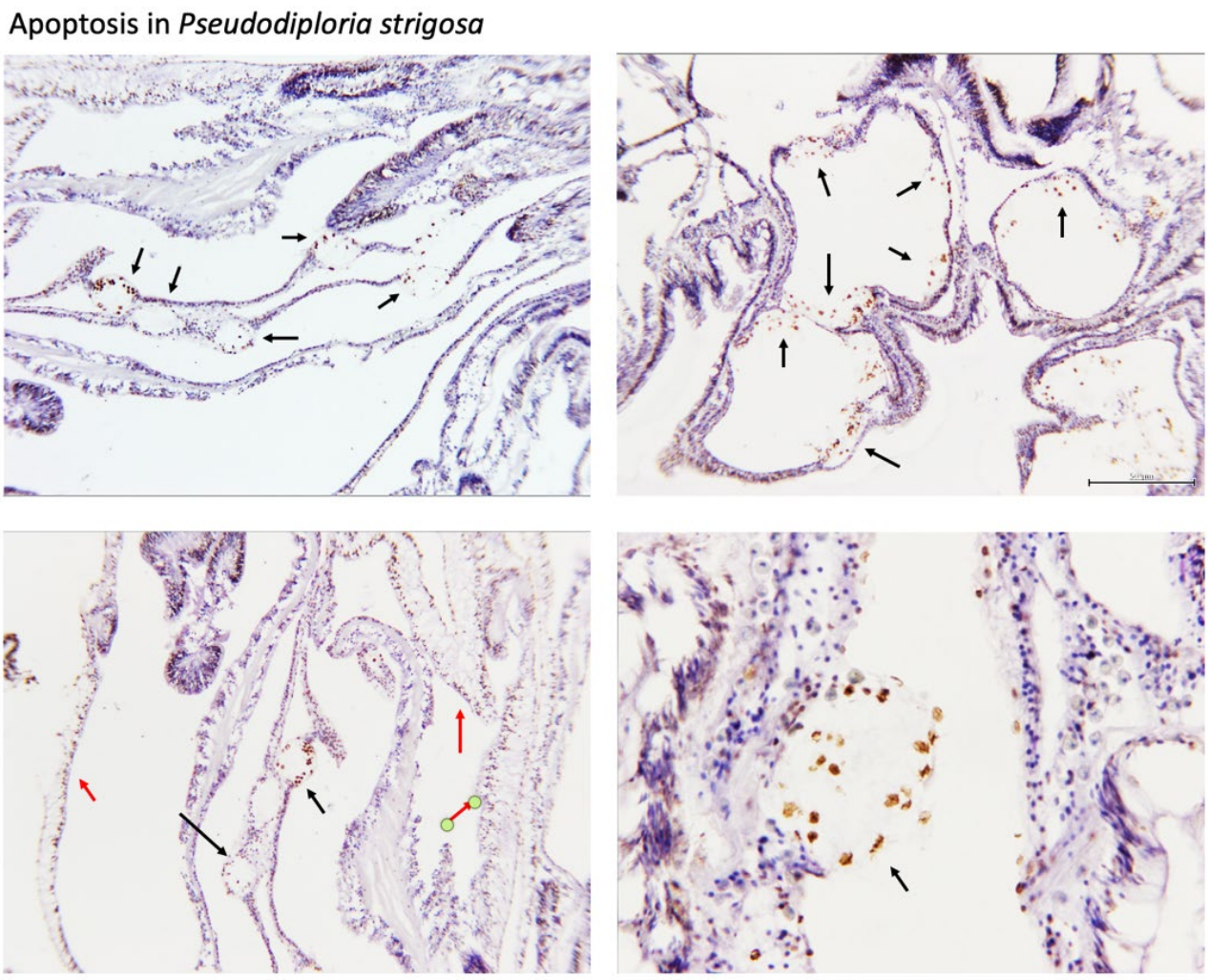

Figure 14: Apoptosis observed to be lining areas of tissue rupture and necrosis in the SCTLD lesion of *Pseudodiploria strigosa*. Orange-brown staining indicates apoptotic cells, blue staining indicates intact nuclei. Black arrows point to areas of tissue rupture and accompanying apoptosis, red arrows point to areas of apoptosis in a swollen basal body wall (BBW).

4.2. Task 2

Microscopy analysis of the 2016 FWRI slides has so far shown abundant necrosis and degradation of algal cells within apparently healthy, diseased, and unaffected samples. **Comparing diseased and unaffected slides from the same colony did not give any indication as to which, if any, pathological sign was the first to display.** Supposedly healthy samples also displayed histopathological signs associated with SCTLD, such as liquefactive necrosis. In almost all cases, multiple forms of necrosis and degradation was present on each photomicrograph. Vacuolation was most common, with severity corresponding with algal health. Areas with severe vacuolation often had swollen or pyknotic algal cells as well indicating the symbiosome as a whole has some effect in pathology. Pyknotic necrosis was more common than swelling in all health types. Algal cells showed cell wall disintegration most commonly in areas where the gastrodermis had begun or completely detached from the mesoglea. Similarly, areas directly next to LN also showed algal

abnormalities. LN was most common in the gastrodermis, although the lesion did affect the mesoglea and epidermis in a small number of micrographs examined. In summary, understanding the histopathological signs displayed by algal cells affected by SCTLD will take time and the examination of a large number of replicates. Finishing the 2017–2018 FWRI samples may provide further evidence as to whether a pattern is followed in how histopathological signs present.

Dinoflagellate counts were only completed on a small number of slides due to lab closures caused by the COVID-19 Pandemic. More data are needed to see how SCTLD affects zooxanthellae numbers and reproduction. **Due to the small sample size, no real conclusions can be drawn at this time.** Initial results do indicate though that diseased samples have a thicker

gastrodermis. This is most likely from expansion due to vacuolation and the early stages of liquefactive necrosis. When cell counts have been completed, a better understanding of dinoflagellate loss and reproduction in SCTLD affected samples may give a better understanding of their role over the course of the disease.

Completing the current dinoflagellate counts and analysis should be prioritized. Not enough information has been collected to understand what is happening within the zooxanthellae themselves and in the surrounding symbiosome. Better histopathological understanding of these symbionts is needed to compliment other ongoing forms of research. By creating a spatial awareness of what is occurring within the tissue itself, a better overall understanding of the disease is more likely. The continued work with the FWRI samples as well as the collaborative effort of the creation of new histoslides from cores that target specific classifications of zooxanthellae with Dr. Andrew Baker's lab will help create a foundation of understanding of the relationship that dinoflagellates have with SCTLD.

4.3. Task 3

Preliminary results indicated that apoptosis was consistently observed in the tissues of corals affected by SCTLD, suggesting that this mode of cell death is involved in SCTLD pathology. In many cases, apoptosis was seen to coincide with other signs of disease, such as instances of necrosis, tissue-layer rupture, dissociated gastrodermis, vacuolation of zooxanthellae, and swelling of the basal body wall. Additional samples and further analysis are needed to fully describe the interplay between the mechanism of cell death and other histological indicators of SCTLD. **When all samples have been processed for immunohistochemistry, further analysis will uncover any relationships between the morphological signature of SCTLD histopathology and apoptosis to determine how this mode of cell death might be involved.**

Although apoptosis was consistently observed to be abundant in areas displaying signs of disease, apoptosis was also abundant in tissue with no apparent lesion. This may possibly suggest that apoptosis is an early indicator of disease and is expressed in tissues before they begin to morphologically degrade. **Further analysis is needed to discern the precise role of this immune response in SCTLD pathology, i.e., whether apoptosis is being expressed ahead of the disease lesion as an appropriately-regulated immune response by the coral host, or whether the degree of apoptosis preceding lesions is indicative of an "apoptotic cascade" that results from the pathological dysregulation of this pathway.** The continuation of this

project will analyze the full sample set to better describe the series of clinical developments in SCTLD as it relates to this process. **We also suggest expanding the scope of this analysis to include any samples that result in time-series experiments aimed at documenting the sequential development of SCTLD in coral tissues to capture the earliest expression of apoptosis and how that might influence further signs of lesion development**. This will help us to understand whether apoptosis is ultimately driving the rapid tissue loss associated with the SCTLD lesion and how the corals' own immune mechanisms may be contributing to this lethal disease.

Apoptosis was abundant in the one apparently healthy coral colony (showing no gross signs of SCTLD) that was tested so far. It is possible that this is indicative of immune activity as the coral responds to exposure to the SCTLD pathogen(s) or some other stressor(s). If apoptosis is found to be an early indicator of SCTLD, it is also possible that the earliest stages of disease were captured in this sample before a gross lesion became visible. However, the background rates of cell turnover in coral tissues are currently unknown, but these are epithelial cells that have a limited lifespan and probably require continuing replacement similar to the cells of mammalian respiratory and gastrointestinal epithelium (Green 2011). Further analysis is needed to determine the normal range of apoptosis expression in optimally functioning coral epithelia. **Additional samples of healthy corals will be processed to confirm this observation and to determine the extent to which seemingly healthy coral tissues exhibit this response.**

5. LITERATURE CITED

Apprill, A., McNally, S., Parsons, R., & Weber, L. (2015). Minor revision to V4 region SSU rRNA 806R gene primer greatly increases detection of SAR11 bacterioplankton. Aquatic Microbial Ecology, 75. https://doi.org/10.3354/ame01753

Callahan, B. J., McMurdie, P. J., & Holmes, S. P. (2017). Exact sequence variants should replace operational taxonomic units in marker-gene data analysis. The ISME Journal, 11(12), 2639–2643. https://doi.org/10.1038/ismej.2017.119

Callahan, B. J., McMurdie, P. J., Rosen, M. J., Han, A. W., Johnson, A. J. A., & Holmes, S. P. (2016). DADA2: High-resolution sample inference from Illumina amplicon data. Nature Methods, 13(7), 581–583. https://doi.org/10.1038/nmeth.3869

Clode, P. L., Saunders, M., Maker, G., Ludwig, M., & Atkins, C. A. (2009). Uric acid deposits in symbiotic marine algae. Plant, Cell & Environment, 32(2), https://doi.org/10.1111/j.1365-3040.2008.01909.x

Gardes, M., and Bruns, T. D. (1993). ITS primers with enhanced specificity for basidiomycetes-application to the identification of mycorrhizae and rusts. Molecular Ecology 2(2), 113–118.

Garrity, M. M., Burgart, L. J., Riehle, D. L., Hill, E. M., Sebo, T. J., & Witzig, T. (2003). Identifying and quantifying apoptosis: Navigating technical pitfalls. Modern Pathology, 16(4), 389–394. https://doi.org/10.1097/01.MP.0000062657.30170.92

Green, D. (2011). Means to an End: Apoptosis and Other Cell Death Mechanisms. Cold Spring Harbor Laboratory Press, Maine.

Katoh, K., Misawa, K., Kuma, K., & Miyata, T. (2002). MAFFT: A novel method for rapid multiple sequence alignment based on fast Fourier transform. Nucleic Acids Research, 30(14), 3059–3066.

Parada, A. E., Needham, D. M., & Fuhrman, J. A. (2016). Every base matters: Assessing small subunit rRNA primers for marine microbiomes with mock communities, time series and global field samples. Environmental Microbiology, 18(5), 1403–1414. https://doi.org/10.1111/1462-2920.13023

Precht, W. F., Gintert, B. E., Robbart, M. L., Fura, R., & van Woesik, R. (2016). Unprecedented disease-related coral mortality in southeastern Florida. Scientific Reports 6, 31374, https://doi.org/10.1038/srep31374

Rasband, W. S. (2020). ImageJ, U. S. National Institutes of Health, Bethesda, Maryland, USA, https://imagej.nih.gov/ij/, 1997-2018

Walton, C. J., Hayes, N. K., & Gilliam, D. S. (2018). Impacts of a Regional, Multi-Year, Multi-Species Coral Disease Outbreak in Southeast Florida. Frontiers in Marine Science, 5. https://doi.org/10.3389/fmars.2018.00323

White, T. J., Bruns, T., Lee, S. J. W. T., and Taylor, J. L. (1990). Amplification and direct sequencing of fungal ribosomal RNA genes for phylogenetics. PCR Protocols: A Guide to Methods and Applications, 18(1), 315-322.